國立臺灣大學理學院物理學研究所

博士論文

Graduate Institute of Physics
College of Science
National Taiwan University

Doctoral Dissertation

準粒子凝聚態在二維系統與自旋有序之應用

Quasi-particle Condensation in Two-Dimensional System and Its Application in Spin Ordering

研究生：陳志宇

Chih-Yu Chen

指導教授：胡崇德 博士

Supervisor: C.D. Hu, Ph.D.

中華民國 108 年 7 月

July, 2019

doi:10.6342/NTU201901151

國立臺灣大學博士學位論文
口試委員會審定書

準粒子凝聚態在二維系統與自旋有序之應用
Quasi-particle Condensation in Two-Dimensional System and Its Application in Spin Ordering

本論文係陳志宇君（D99222003）在國立臺灣大學物理學系、所完成之博士學位論文，於民國 108 年 06 月 18 日承下列考試委員審查通過及口試及格，特此證明

口試委員：

胡崇德 （簽名）	
張慶瑞（指導教授）	
雒振詩	
陳繩義	
林育中	

誌謝

首先感謝我的指導教授胡崇德老師，給我充實的博士生涯，以及口試委員張慶瑞老師，林育中老師，程思誠教授，陳繩義教授的指教。

再來感謝我的家人，父母，妻子怡菱，女兒玉紓，謝謝你們容忍一個 30 幾歲還不賺大錢的任性兒子老公爸爸，大力相挺讓我無後顧之憂完成學位。還有各位關心我的親戚們。

三感謝我的各位好朋友們，長洪武術的師母，小圈圈練功團的師兄弟，聆聽唱片的好朋友們與前輩，3，感謝你們讓生活充滿豐富內涵，當喜怒哀樂的出口。

最後感謝我的三位導師陳清河，林主惟與黃義忠先生，你們影響是一生的。

doi:10.6342/NTU201901151

中文摘要

準粒子凝聚態在凝態物理的應用廣泛，在玻色-愛因斯坦凝聚，超導體與超流體中扮演重要角色。本論文主要分為兩部分，第二至第六章討論二維半導體中激子（exciton）的凝聚態，研究顯示一種新的混合態波函數為二維半導體激子凝聚態的基態，並提供可能的實驗量測方式。

第七至第十章研究磁振子（magnon）的凝聚態，組織現有的 Schwinger-boson 平均場理論，應用於氧化銅材料，以及討論動量非零之玻色-愛因斯坦凝聚態之物理意義與氧化銅中 commensurate-incommensurate 相變生成之可能之微觀機制。

關鍵字：激子、二維半導體、玻色-愛因斯坦凝聚、氧化銅、磁振子、自旋、孤立子

doi:10.6342/NTU201901151

ABSTRACT

In this thesis, we study the aspects of quasiparticle condensate phenomena. The Bose-Einstein condensation of quasiparticle plays an important role in many areas such as the superconductivity, superfluidity, magnons, polaritons, and of course, one of the main topic of this thesis-exciton. The exciton condensation of two-dimensional (2D) semiconductors is reports in Ch. 2-6. We start from an effective Hamiltonian of 2D semiconductors and show an interesting mixed state of exciton condensate.

The bosonization of electrons can also be a useful mathematical tool to study quantum spin systems. In Ch. 7-10, we extend the Schwinger boson mean field theory (SBMFT) method of ferromagnetic and antiferromagnetic systems. The condensation of Schwinger bosons can describe the ordering phase of spins. We study the commensurate-incommensurate phase transition of CuO as an example.

Key words: exciton, 2D semiconductor, Bose-Einstein condensation, CuO, magnon, commensurate-incommensurate phase transition, soliton

doi:10.6342/NTU201901151

CONTENTS

CONTENTS

doi:10.6342/NTU201901151

doi:10.6342/NTU201901151

LIST OF FIGURES

doi:10.6342/NTU201901151

doi:10.6342/NTU201901151

LIST OF TABLES

doi:10.6342/NTU201901151

Quasi-particle Condensation in Two-Dimensional System and Its Application in Spin Ordering

Chih-Yu Chen
Supervisor: C.D. Hu

July 2, 2019

doi:10.6342/NTU201901151

doi:10.6342/NTU201901151

Contents

doi:10.6342/NTU201901151

doi:10.6342/NTU201901151

Chapter 1

Exordium

Cooper pairs and Bose-Einstein condensation (BEC) are two very profound quantum states. They have common properties and important differences. The former is the origin of the celebrated superconductivity and BEC is the cause of fascinating superfluidity. On the other hand, the fact that Cooper pairs are formed by fermions and BEC are composed of bosons engenders far-reaching different physical consequences.

Let's start with superconductors [1]. The physical properties of superconductivity can be described microscopically by BCS theory. In BCS theory, a key idea is electron–electron will form a pair (Cooper pair) in superconductors. More precisely, two electrons near Fermi surface can form pairs via electron-phonon interaction as temperature is lower than some critical value T_c.

Bose-Einstein condensation (BEC) of bosons is a state of matter which a large fraction of bosons occupy the lowest quantum state. This phenomena is first predicted by S.N. Bose in 1924 and later extended by A. Einstein in 1924 to 1925. The experimental discovery of BEC in dilute gas at low temperature in 1995 by W. Ketterle, E. Cornell and C. Wieman [2, 3]. In condensate state, microscopic quantum phenomena, particularly wave-function interference, become apparent macroscopically. We can say the condensation of bosons is "conventional" since the statistical and spin nature of boson allows the condensation phase. On the other hand, fermions cannot occupy the ground sate with a great amount because the Pauli exclusion principle.

In general, the wave-function of BEC centers at zero momentum since intuitively zero momentum is the lowest energy state. The finite momentum BEC of strongly interacting Bose system is discussed by Yukalov [5]. This phenomena has also been discussed in the past decade in magnon system, see for example, [6, 7]. That is, the condensate state occurs at some finite $\mathbf{k} = \mathbf{k}_0$. Its properties of breaking $U(1)$ symmetry of Helium III is discussed

doi:10.6342/NTU201901151

in the work of Bunkov and Volovik [8]. In the article of Kohn and Sherrington [4], they classified bosons in two types. Quoting results are shown in Table 1.1 and Table 1.2.

Apart from the conventional BEC of bosons, the quasi-particles as bosons have more complex and interesting contents, especially for the type 2 condensates. It allows possibility of the finite momentum Bose-Einstein condensation which is usually to be zero. We keep Table 1.1 of single boson for comprehensiveness however we will focus on the condensation of quasi-particles summarized in Table 1.2. One needs to bear in mind that some systems may display both type 1 and type 2 mixed situation. For example the crystalline superconductor may be viewed as type 1 bosons (Cooper pair), in a condensate of type 2 bosons (the normal host crystal).

Looking back to the magnon system [6, 7]. One more question rises: Are magnons type 2 bosons? In the work of J. Hick *et. al.*, they derived an effective boson Hamiltonian to describing the lowest magnon band of YIG, see Appendix of ref. [7]. They used method developed by Holstein and Primakoff in 1940 which can be found in original paper or other literature [9]. Such boson derived from spins leads no superfluidity but its condensation offers a view point in dealing magnetic ordering system. The Schwinger boson mean field theory (SBMFT), a method of dealing with electron spins, also applies similar idea as that which we are going to use of Holstein-Primakoff bosonization.

The main purpose of this thesis is to present condensation of type 2 bosons on the platform of real physical systems. The exciton condensation of two-dimensional (2D) semiconductors is reported in PART II. We start from an effective Hamiltonian of 2D semiconductors and show an interesting mixed state of exciton condensate. In PART III, we extend the SBMFT of ferromagnetic and antiferromagnetic systems. The bosonization of electron spins can also be a useful mathematical tool to study quantum spin systems. BEC of Schwinger bosons can describe the ordering phase of spins. We also study the commensurate-incommensurate phase transition of CuO as an example.

doi:10.6342/NTU201901151

single bosons	**type 1**	**type 2**
examples	^{4}He atoms, tightly bounded fermions	exciton
nature	complexes of even number of real fermions	particle-hole bound complexes
form of Green's functions and density matrices	singular as functions of momentum **sum** variables	singular as functions of momentum **difference** variables
momentum properties	carry mechanical momentum	may or may not carry mechanical momentum

Table 1.1: Copy from Table 1 of Kohn and Sherrington's review article [4]. The properties of two types of single bosons

condensed states	**type 1**	**type 2**
example	He II	excitonic phase
type of additional order	**off-diagonal** long-range order	**diagonal** long-range order
superfluidity	yes	no
form of Green's functions and density matrices	macroscopic singularities as functions of momentum **sum** variables	macroscopic singularities as functions of momentum **difference** variables

Table 1.2: Copy from Table 2 of Kohn and Sherrington's review article [4]. The properties of two types of condensate states.

doi:10.6342/NTU201901151

doi:10.6342/NTU201901151

Chapter 2

Introduction of Exciton Condensate

Electrons in semiconductors can form quasi-particle states. The binding of an electron and a hole by attractive Coulomb interaction gives rise to an exciton. If the density is high enough, the overlap of excitons becomes significant. At low-enough temperature they form condensate and their collective behaviors such as Andreev reflection [10], superradiance [11] and Josephson tunneling [12] are similar to those of the Cooper pairs in superconductors.

The investigation of condensed phase of excitons has made great progress in the past few decades [13]. The theoretical scheme for condensation phase and collective behaviors was constructed by pioneer works of Kozlov *et al.* [14, 15]. They pointed out in a crystal with closely-lying bands the Coulomb interaction became important. At low temperature, the density of excitons can be very high. Once condensed, the gap function $\Delta_{\mathbf{k}}$ becomes finite and the system enters a BCS-like state. Later, the theory of exciton condensation in bulk germanium and silicon is discussed by the work of M. Combescot and P. Nozières [16]. Their results were in good agreement with experiments in aspects of ground state energy and critical density. The two-dimensional (2D) exciton instability in an InAs-GaSb-based system has been reported by Naveh and Laikhtman [17]. They formulated the gap equation of exciton condensation in their case I where electrons and holes are separated and compared it with that of BCS theory. They also discussed how electric field effects the density of condensation. The electron-hole system of InAs-GaSb bi-layers is also discussed recently by Pikulin and Hyart [18]. They study small tunneling and large tunneling between layers in which the systems display s-wave exciton condensation and quantum spin Hall (QSH) insulator property, respectively. This QSH insulator phase exhibits topological nontrivial property with p-wave exciton parameter. Despite these interesting

doi:10.6342/NTU201901151

properties, however, the exciton condensation in single-layer materials is still an issue which needs more investigation.

After the discovery of graphene [19], more and more 2D materials have been synthesized. Silicene (2D silicon) and germanene (2D germanium) [20, 21] will be discussed in this work. These low-bulked honeycomb materials have topological properties related to QSH effect. The existence of QSH effect in 2D system was first proposed by Kane and Mele in graphene [22]. They showed the band gap can be opened by spin-orbit coupling (SOC). However, the first order SOC is shown to be rather weak in subsequent works [23, 24]. Hence the QSH effect of graphene can only happen at incredibly low temperature. On the other hand, low-bulked 2D semiconductors of heavier elements have much stronger SOC [20, 23]. Furthermore, it was shown that p-wave superconductivity could be stable in a 2D system with Rashba interaction [25, 26]. These works give us motivation to study the combination of exciton condensation and 2D semiconductors.

In chapter 2-6, we will discuss some interesting physical results owing to SOC. We also take one step further to discuss the system under effect of external electric field. Our study shows that the SOC, intrinsic or extrinsic, plays an important role in exciton condensation in 2D materials. The latter clearly favors the mixed states of s-wave and p-wave. Chapter 2-6 is organized as follows. Chapter 2 is the introduction of exciton condensation of semiconductors. In Ch.3, we discuss the effective Hamiltonian considering SOC and Rashba interaction. It gives the theoretical basis of this paper. In Ch.4, we discuss the Coulomb interaction in details. The consideration of spin configurations and characters of bands are of great importance. In Ch.5, we derive the gap equation of exciton condensation, which is the central equation of exciton condensaiton. We then show that the exciton condensation should be formed in p-wave-like state due to the mixed state nature of spins. Experiments are proposed to verify such state in Ch.6.

doi:10.6342/NTU201901151

Chapter 3

Effective Hamiltonian of 2D Semiconductors

In this chapter, we demonstrate the effective Hamiltonian of silicene and germanene. The cases with and without external electric field are presented in part A. and part B, respectively. The band structures and eigenstates are also calculated. Silicene and germanene have honeycomb crystal structure from top view which is similar to graphene. They have a zig-zag geometry from side view. That is, the sublattice A and B are not coplanar but they are still 2D systems. In the work of C.C. Liu *et al.* [27], they proposed an effective low energy Hamiltonian of 2D semiconductors.

3.1 The effective Hamiltonian without external field

The obtained Hamiltonian around **K** in crystal momentum space for low-energy states $(\phi_{1\uparrow}, \phi_{1\downarrow}, \phi_{4\uparrow}, \phi_{4\downarrow})$ is

$$H_0^{band} = (\epsilon_1 - \lambda_{so}^{2nd})I_4 + \begin{pmatrix} h_{11} & v_F k_+ I_2 \\ v_F k_- I_2 & -h_{11} \end{pmatrix}, \tag{3.1}$$

where

$$h_{11} = -\lambda_{so}\sigma_z - a\lambda_R(k_y\sigma_x - k_x\sigma_y), \tag{3.2}$$

I_4 and I_2 are 4×4 and 2×2 identity matrices, respectively. σ_i is the Pauli matrix for spins and a is the lattice constant of 2D semiconductors. Eq. (3.1)

doi:10.6342/NTU201901151

is in the representation of the low-energy states ϕ_1 and ϕ_4

$$\begin{aligned}|\phi_1\rangle &= u_{11}\left|p_z^A\right\rangle + u_{21}\left|s^A\right\rangle + \frac{u_{31}}{\sqrt{2}}(\left|p_x^B\right\rangle - i\left|p_y^B\right\rangle),\\ |\phi_4\rangle &= u_{11}\left|p_z^B\right\rangle - u_{21}\left|s^B\right\rangle - \frac{u_{31}}{\sqrt{2}}(\left|p_x^A\right\rangle + i\left|p_y^A\right\rangle),\end{aligned} \tag{3.3}$$

where u_{11}, u_{21} and u_{31} are normalized coefficients. One can find details in Ref. [27] and we here simply treat them as coefficients of linear combination of states. Superscripts A and B denote two sublattices of the honeycomb lattice. The complete basis are the direct product of orbitals and spins $\left|\phi_{1(4)}\right\rangle \otimes |\uparrow(\downarrow)\rangle$. λ_R is the strength of internal Rashba interaction, $\lambda_{so} = \lambda_{so}^{1st} + \lambda_{so}^{2nd}$ where λ_{so}^{1st} and λ_{so}^{2nd} are the two kinds of spin-orbit interactions considered in (25) and (30) of Ref. [27]. v_F is the Fermi velocity and the relation to the tight-binding potentials are given by (22) of Ref. [27].

Silicene and germanene have different physical properties from graphene due to the low-buckled geometry. The most important is it gives rise to two directions of SOC. One lies on the honeycomb plane, which appears in graphene as well. The other is perpendicular to the plane in the form of $-it_1\mu_{ij}(\vec{\sigma}\times\vec{d}_{ij}^{\,0})_z$, see (4) of Ref. [27]. The other geometry induced interaction is the intrinsic Rashba interaction $a\lambda_R$, which is much weaker than the SOC, see Eq. (39) of [27]. In this work, we first simplify the notations by letting $r \equiv a\lambda_R$ and $\lambda \equiv \lambda_{so}$ to avoid unnecessary complications. The degenerate eigenvalues of H_0^{band} are $\pm\epsilon_{\mathbf{k}}$ where

$$\epsilon_{\mathbf{k}} = \sqrt{(r^2 + v_F^2)k^2 + \lambda^2}. \tag{3.4}$$

As we can see from Eq.(3.4), 2λ represents the energy gap between valence band and conduction band at momentum $\mathbf{K}$. The band gap E_g is 2λ. With eigenvalues given by Eq. (3.4), we have four eigenvectors

$$\begin{pmatrix} b_1\\ b_2\\ a_1\\ a_2\end{pmatrix} = \frac{1}{\sqrt{M_k}}\begin{pmatrix} A_k & B_k & 1 & 0\\ 0 & 1 & -B_k^* & A_k^*\\ C_k & -A_k & 0 & 1\\ 1 & 0 & -A_k^* & C_k\end{pmatrix}\begin{pmatrix}\phi_{1\uparrow}\\ \phi_{1\downarrow}\\ \phi_{4\uparrow}\\ \phi_{4\downarrow}\end{pmatrix}, \tag{3.5}$$

where

$$A_{\mathbf{k}} = \frac{\epsilon_{\mathbf{k}} - \lambda}{v_F k_-} \qquad B_{\mathbf{k}} = \frac{irk_+}{v_F k_-} \qquad C_{\mathbf{k}} = \frac{-ir}{v_F}, \tag{3.6}$$

and $M_k = [(\epsilon_k - \lambda)^2 + k^2(r^2 + v_F^2)]/(kv_F)^2$ is nothing but the normalization of eigenvectors. b_1 and b_2 are conduction bands since they both have energy $+\epsilon_{\mathbf{k}}$ whilst a_1 and a_2 are valence bands which are of energy $-\epsilon_{\mathbf{k}}$. Thus we have a band structure with two degenerate conduction bands and two degenerate valence bands, see FIG. 3.1(a) where the parameters of germanene are used.

doi:10.6342/NTU201901151

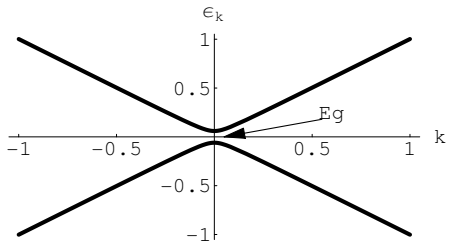

(a)

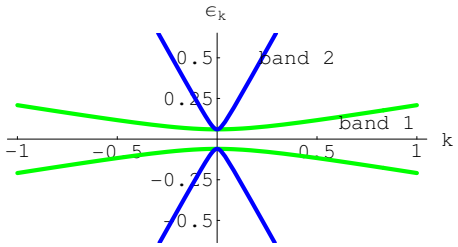

(b)

Figure 3.1: (a) Two-fold degeneracy in valence and conduction bands *without* external field. (b)Minus mode (bands 1, green) and plus mode (bands 2, blue) *with* external field $R = 1.2v_F$.

3.2 The effective Hamiltonian with external field

Now we consider the system in an external electric field $E_z\hat{z}$ which is perpendicular to the 2D xy plane. The induced Rashba interaction becomes $R(k_y\sigma_x - k_x\sigma_y)$, where R is the Rashba parameter which is proportional to E_z [28]. In the example given in FIG. 3.1(b), $R = 1.2v_F$ means that we need an electric field of energy about 0.92eV per lattice cite of germanene [27], which is 0.23eV·Å. In practice, we can reach this by adding a gate voltage in the magnitude of order 10V [29]. One can see the change of the Rashba constant due to the gate voltage. Though the effect depends on properties of materials, the order of magnitude should be the same and it is very promising to achieve in laboratory. With the basis $(\phi_{1\uparrow}, \phi_{1\downarrow}, \phi_{4\uparrow}, \phi_{4\downarrow})^T$, the effective Hamiltonian at **K** point is

$$H_1^{band} = (\epsilon_1 - \lambda_{so}^{2nd})I_4 + \begin{pmatrix} h_{11} & v_F k_+ I_2 \\ v_F k_- I_2 & h'_{11} \end{pmatrix}, \tag{3.7}$$

where $h_{11} = -\lambda_{so}\sigma_z - R(k_y\sigma_x - k_x\sigma_y)$, and $h'_{11} = \lambda_{so}\sigma_z - R(k_y\sigma_x - k_x\sigma_y)$. In contrast to the effective Hamiltonian without external field, the lower right hand corner is not $-h_{11}$. The difference is caused by the formation of Rashba interaction. The Rashba interaction of the case without external

doi:10.6342/NTU201901151

field is intrinsic, which has opposite directions on A and B sites. The Rashba interaction due to the external field, on the contrary, has the same direction on A and B sites and it can be much stronger than the intrinsic one. The external field breaks the mirror symmetry of internal Rashba interaction. The eigenvalues of Hamiltonian (3.7) are $\pm\epsilon_{1\mathbf{k}}$ with

$$\epsilon_{1\mathbf{k}} = \sqrt{\lambda^2 + k^2(R - v_F)^2}, \tag{3.8}$$

and $\pm\epsilon_{2\mathbf{k}}$ with

$$\epsilon_{2\mathbf{k}} = \sqrt{\lambda^2 + k^2(R + v_F)^2}. \tag{3.9}$$

The degeneracy is lifted, see FIG. 3.1(b). The bands with $R+v_F$ and $R-v_F$ are in blue and green, respectively. The band 1, with $\epsilon_{1\mathbf{k}}$, has the smaller magnitude. Only at $k = 0$, the bottoms of two conduction bands and tops of two valence bands touch each other, and the energy gap is still of magnitude 2λ at $k = 0$. We then solve for the eigenvectors. For energy $\pm\epsilon_{1\mathbf{k}}$,

$$b_1' = \frac{1}{n_1}\begin{pmatrix} -ik(R - v_F) \\ \frac{k_+}{k}(\epsilon_{1\mathbf{k}} + \lambda) \\ \frac{ik_-}{k}(\epsilon_{1\mathbf{k}} + \lambda) \\ -k(R - v_F) \end{pmatrix}, \quad a_1' = \frac{1}{n_1}\begin{pmatrix} i(\epsilon_{1\mathbf{k}} + \lambda) \\ k_+(R - v_F) \\ ik_-(R - v_F) \\ \epsilon_{1\mathbf{k}} + \lambda \end{pmatrix}. \tag{3.10}$$

For energy $\pm\epsilon_{2\mathbf{k}}$, we have

$$b_2' = \frac{1}{n_2}\begin{pmatrix} -ik(R + v_F) \\ \frac{k_+}{k}(\epsilon_{2\mathbf{k}} + \lambda) \\ \frac{ik_-}{k}(\epsilon_{2\mathbf{k}} + \lambda) \\ k(R + v_F) \end{pmatrix}, \quad a_2' = \frac{1}{n_2}\begin{pmatrix} -i(\epsilon_{2\mathbf{k}} + \lambda) \\ -k_+(R + v_F) \\ ik_-(R + v_F) \\ \epsilon_{2\mathbf{k}} + \lambda \end{pmatrix}. \tag{3.11}$$

Similar to a_i and b_i before, b_i' and a_i' correspond to conduction band and valence band states, respectively. The normalization factor is $n_i = 2\sqrt{\epsilon_{i\mathbf{k}}(\epsilon_{i\mathbf{k}} + \lambda)}$. Hence, in the tight-binding model, the Hamiltonian with external field can still be diagonalized.

doi:10.6342/NTU201901151

Chapter 4

Coulomb Interaction Revisit

4.1 Spin selection rule and 2D Coulomb potential

In this section, we first discussed the Coulomb interaction in a 2D system and paid special attention to spin configurations. Analogous to the interacting fermions in BCS theory, where the interaction leads to Cooper pairs in superconductors, attractive Coulomb interaction between electrons and holes plays a crucial role in forming the exciton condensate state. We consider a comprehensive Hamiltonian of an electronic system

$$H_i = H_i^{band} + V \tag{4.1}$$

where H_i^{band} is the effective Hamiltonian in Eq. (3.1) or Eq. (3.7) under the representation of basis $(\phi_{1\uparrow}, \phi_{1\downarrow}, \phi_{4\uparrow}, \phi_{4\downarrow})^T$. Index $i = 0$ and $i = 1$ represent the cases without and with external field, respectively. The Coulomb term is

$$V = \frac{1}{2} \sum_{ijmn} \sum_{\mathbf{k},\mathbf{k}',\mathbf{q}} \sum_{\sigma\sigma'} \langle \mathbf{k}+\mathbf{q}, i; \mathbf{k}', j | V_{\mathbf{q}} | \mathbf{k}'-\mathbf{q}, m; \mathbf{k}, n \rangle \, c^\dagger_{i,\mathbf{k}+\mathbf{q},\sigma} c^\dagger_{j,\mathbf{k}'-\mathbf{q},\sigma'} c_{m,\mathbf{k}',\sigma'} c_{n,\mathbf{k},\sigma}. \tag{4.2}$$

Operator c's represent ϕ_1 or ϕ_4 with i, j, m and n being either 1 or 4, (see Eq. (3.3)), and σ and σ' are spin indices. The effective two-dimensional Coulomb potential in momentum space [30] is

$$V_{\mathbf{q}} = \frac{2\pi e^2}{|\mathbf{q}|(1 + 2\pi\alpha_{2D}|\mathbf{q}|)}, \tag{4.3}$$

where α_{2D} is the 2D polarizability caused by electron screening of bands. The magnitude of α can be calculated by Eq. (10) of Ref. [31]

$$\alpha_{2D} = \frac{e^2}{2\pi} \left(-\frac{1}{E_g + x} \right) \Big|_0^{x_M}. \tag{4.4}$$

doi:10.6342/NTU201901151

x_M is the energy of the state at the first Brillouin zone boundary. For germanene, $x_M \approx 25E_g$ in the case without external field. On the other hand, x_M is about $6.25E_g$ for band 1 and much larger ($\sim$50 times) than E_g for band 2 as $R = 1.2v_F$, see FIG. 3.1(b).

Same as the work in Ref. [32], we only consider the Coulomb interaction between even numbers of the electrons in valence bands and conduction bands. That is, terms like $b^\dagger a^\dagger aa$ or $b^\dagger a^\dagger bb$ are omitted since they contribute little to exciton pairing. In our 2D system described by H_i^{band} the eigenvectors are spin mixed states and Coulomb interaction doesn't change spins. Hence, we start with the Coulomb interaction in ϕ representation then extract out the coefficients of operators $b^\dagger a^\dagger ab$, $b^\dagger a^\dagger ba$ because the spin configurations are clearer in ϕ representation. Eq. (4.2) in momentum space is written in the second quantization form

$$\frac{1}{2}\sum_{ijmn}\sum_{\mathbf{k},\mathbf{k'},\mathbf{q},\sigma\sigma'} V_{\mathbf{q}}^{ijmn}((1-\delta_{\sigma\sigma'})c^\dagger_{i,\mathbf{k}+\mathbf{q},\sigma}c^\dagger_{j,\mathbf{k'}-\mathbf{q},\sigma'}c_{m,\mathbf{k'},\sigma'}c_{n,\mathbf{k},\sigma}+ \delta_{\sigma\sigma'}c^\dagger_{i,\mathbf{k}+\mathbf{q},\sigma}c^\dagger_{j,\mathbf{k'}-\mathbf{q},\sigma'}c_{n,\mathbf{k'},\sigma'}c_{m,\mathbf{k},\sigma}), \tag{4.5}$$

In (4.5), the first term is the direct term and the second contains the exchange term. The possible spin configurations $(\sigma\sigma'\sigma'\sigma)$ are $(\uparrow\uparrow\uparrow\uparrow), (\downarrow\downarrow\downarrow\downarrow), (\uparrow\downarrow\downarrow\uparrow)$ and $(\downarrow\uparrow\uparrow\downarrow)$. Coulomb interaction in momentum representation for direct terms and exchange terms are proportional to $(|\mathbf{k}-\mathbf{k'}| + 2\pi\alpha_{2D}|\mathbf{k}-\mathbf{k'}|^2)^{-1}$ and $(|\mathbf{k}-\mathbf{k'}+\mathbf{q}| + 2\pi\alpha_{2D}|\mathbf{k}-\mathbf{k'}+\mathbf{q}|^2)^{-1}$, respectively. Since the screening effect is dominant, electrons with all parallel spins give negligible contribution since direct and exchange terms approximately cancel each other. In summery, only spin configurations $(\uparrow\downarrow\downarrow\uparrow)$ and $(\downarrow\uparrow\uparrow\downarrow)$ survive.

Furthermore, the overlap of wavefunction ϕ_1 and ϕ_4 is small according to Eq. (3.3). This is owing to the small overlap of $|p_z\rangle$ and $|p_x\rangle + i\,|p_y\rangle$ orbitals and that between wave functions of different sublattices (A and B). The summations such as $\sum_{\mathbf{k},\mathbf{k'},\mathbf{q}} V_{\mathbf{q}}^{1114}\phi^\dagger_{1,\mathbf{k}+\mathbf{q}\uparrow}\phi^\dagger_{1,\mathbf{k'}-\mathbf{q}\downarrow}\phi_{1,\mathbf{k'}\downarrow}\phi_{4,\mathbf{k}\uparrow}$ or $\sum_{\mathbf{k},\mathbf{k'},\mathbf{q}} V_{\mathbf{q}}^{1414}\phi^\dagger_{1,\mathbf{k}+\mathbf{q}\uparrow}\phi^\dagger_{4,\mathbf{k'}-\mathbf{q}\downarrow}\phi_{1,\mathbf{k'}\downarrow}\phi_{4,\mathbf{k}\uparrow}$ can be dropped. Thus, with above arguments, we simply consider eight sets of integrations. They are $(\phi^\dagger_{1\uparrow}, \phi^\dagger_{1\downarrow}, \phi_{1\downarrow}, \phi_{1\uparrow})^T$, $(\phi^\dagger_{1\uparrow}, \phi^\dagger_{4\downarrow}, \phi_{4\downarrow}, \phi_{1\uparrow})^T$, $(\phi^\dagger_{4\uparrow}, \phi^\dagger_{1\downarrow}, \phi_{1\downarrow}, \phi_{4\uparrow})^T$, and $(\phi^\dagger_{4\uparrow}, \phi^\dagger_{4\downarrow}, \phi_{4\downarrow}, \phi_{4\uparrow})^T$ and the four others with $\uparrow$ and $\downarrow$ exchanges.

doi:10.6342/NTU201901151

4.2 The form factors of cases with and without external field

According to Eq. (3.5), the inverse transformation of operators $\phi_{i,\sigma}$ with respect to a and b are

$$\begin{pmatrix} \phi_{1\uparrow} \\ \phi_{1\downarrow} \\ \phi_{4\uparrow} \\ \phi_{4\downarrow} \end{pmatrix} = \frac{1}{\sqrt{D_{\mathbf{k}}}k} \begin{pmatrix} (\epsilon_{\mathbf{k}}-\lambda)k_- & 0 & irk^2 & v_F k^2 \\ -irk_-^2 & v_F k^2 & -(\epsilon_{\mathbf{k}}-\lambda)k_- & 0 \\ v_F k^2 & -irk_+^2 & 0 & -(\epsilon_{\mathbf{k}}-\lambda)k_+ \\ 0 & (\epsilon_{\mathbf{k}}-\lambda)k_+ & v_F k^2 & irk^2 \end{pmatrix} \begin{pmatrix} b_1 \\ b_2 \\ a_1 \\ a_2 \end{pmatrix}, \tag{4.6}$$

where $D_{\mathbf{k}} = (\epsilon_{\mathbf{k}}-\lambda)^2 + k^2(r^2+v_F^2)$. A similar equation can be found for the case with external electric field.

We substitute (4.6) into (4.5) and consider the pairing in the same band. That is, terms with $b_1^\dagger a_1^\dagger a_1 b_1$ or $b_2^\dagger a_2^\dagger a_2 b_2$ are kept but terms as $b_1^\dagger a_1^\dagger a_1 b_2$ are excluded. This is because the pairing between different bands is much weaker than that between the same band [33]. The effect of multi-band leads to a form factor $f(\mathbf{k},\mathbf{k}',\mathbf{q})$. As a result, the second quantized Coulomb interaction is of the form

$$\frac{1}{2}\sum_{\mathbf{k},\mathbf{k}'}\left[V_{\mathbf{q}} a^\dagger_{\mathbf{k}+\mathbf{q}} a^\dagger_{\mathbf{k}'-\mathbf{q}} a_{\mathbf{k}'} a_{\mathbf{k}} + V_{\mathbf{q}} b^\dagger_{\mathbf{k}+\mathbf{q}} b^\dagger_{\mathbf{k}'-\mathbf{q}} b_{\mathbf{k}'} b_{\mathbf{k}} + 2f(\mathbf{k},\mathbf{k}',\mathbf{q}) V_{\mathbf{q}} b^\dagger_{\mathbf{k}+\mathbf{q}} a^\dagger_{\mathbf{k}'-\mathbf{q}} a_{\mathbf{k}'} b_{\mathbf{k}}\right], \tag{4.7}$$

where the form factor $f(\mathbf{k},\mathbf{k}',\mathbf{q})$ will be given below in Eqs. (4.10), (4.12) and (4.13). Form factor is not considered in most of the previous works [32, 35]. However, in the case of 2D semiconductors they are important. It has profound effect in determining the forms of the solutions of the gap equation as shown in next section. We treat $f \times V$ as the effective interaction. In the condensed phase, which is the main purpose of this article, a strong correlation between the $\mathbf{k}$ conduction electrons and $-\mathbf{k}$ valence holes is expected. The e-h pairings with zero center-of-mass velocity have the lowest possible kinetic energy. The same approximation is also used in calculation of superconductivity. Hence, we can replace $\mathbf{k}'$ by $\mathbf{k}$ for further simplification:

$$\begin{aligned} &\frac{1}{2}\sum_{\mathbf{k},\mathbf{k}',\mathbf{q}}\left[V_{\mathbf{q}} a^\dagger_{\mathbf{k}+\mathbf{q}} a^\dagger_{\mathbf{k}'-\mathbf{q}} a_{\mathbf{k}'} a_{\mathbf{k}} + V_{\mathbf{q}} b^\dagger_{\mathbf{k}+\mathbf{q}} b^\dagger_{\mathbf{k}'-\mathbf{q}} b_{\mathbf{k}'} b_{\mathbf{k}} + V_{\mathbf{q}} f(\mathbf{k},\mathbf{k}',\mathbf{q}) b^\dagger_{\mathbf{k}+\mathbf{q}} a^\dagger_{\mathbf{k}'-\mathbf{q}} a_{\mathbf{k}'} b_{\mathbf{k}}\right] \\ \approx &\frac{1}{2}\sum_{\mathbf{k},\mathbf{p}}\left[V_{\mathbf{q}} a^\dagger_{\mathbf{k}} a^\dagger_{\mathbf{p}} a_{\mathbf{k}} a_{\mathbf{p}} + V_{\mathbf{q}} b^\dagger_{\mathbf{k}} b^\dagger_{\mathbf{p}} b_{\mathbf{k}} b_{\mathbf{p}} + 2f(\mathbf{k},\mathbf{p}) V_{\mathbf{q}} b^\dagger_{\mathbf{k}} a^\dagger_{\mathbf{p}} a_{\mathbf{k}} b_{\mathbf{p}}\right], \end{aligned} \tag{4.8}$$

doi:10.6342/NTU201901151

where $\mathbf{k}-\mathbf{p}=\mathbf{q}$. Thus we have the two-dimensional exciton Hamiltonian (without external electric field)

$$H_0=\sum_{\mathbf{k}}\epsilon^v_{\mathbf{k}}(a_{1\mathbf{k}}a^\dagger_{1\mathbf{k}}+a_{2\mathbf{k}}a^\dagger_{2\mathbf{k}})+\epsilon^c_{\mathbf{k}}(b^\dagger_{1\mathbf{k}}b_{1\mathbf{k}}+b^\dagger_{2\mathbf{k}}b_{2\mathbf{k}}) + \sum_{\mathbf{k},\mathbf{p}}V_{\mathbf{k}-\mathbf{p}}f_0(\mathbf{k},\mathbf{p})(b^\dagger_{1\mathbf{k}}a^\dagger_{1\mathbf{p}}a_{1\mathbf{k}}b_{1\mathbf{p}}+b^\dagger_{2\mathbf{k}}a^\dagger_{2\mathbf{p}}a_{2\mathbf{k}}b_{2\mathbf{p}}), \tag{4.9}$$

where we consider interband interaction only and absorb the intraband interaction into the band shapes which are obtained by the effective Hamiltonian (3.1). The explicit expression of the form factor f_0 without external field is

$$f_0(\mathbf{k},\mathbf{p})=\frac{(\epsilon_{\mathbf{k}}-\lambda)^2(\epsilon_{\mathbf{p}}-\lambda)^2+k^2p^2v_F^4+2v_F^2(\epsilon_{\mathbf{k}}-\lambda)(\epsilon_{\mathbf{p}}-\lambda)\mathbf{k}\cdot\mathbf{p}}{[(\epsilon_{\mathbf{k}}-\lambda)^2+k^2(r^2+v_F^2)][(\epsilon_{\mathbf{p}}-\lambda)^2+p^2(r^2+v_F^2)]}. \tag{4.10}$$

Notice that in Hamiltonian (4.9), the band labeled 1 and 2 are decoupled so that we can diagonalize the bands separately. They still possess the two-fold degeneracy.

Similarly, in order to discuss the excitons under external field, we express ϕ's in terms of a' and b'.

$$\begin{pmatrix}\phi_{1\uparrow}\\ \phi_{1\downarrow}\\ \phi_{4\uparrow}\\ \phi_{4\downarrow}\end{pmatrix}=\frac{1}{4}\begin{pmatrix}\frac{ik(R-v_F)n_1}{\epsilon_1(\epsilon_1+\lambda)} & \frac{-in_1}{\epsilon_1} & \frac{ik(R+v_F)n_2}{\epsilon_2(\epsilon_2+\lambda)} & \frac{in_2}{\epsilon_2}\\ \frac{k_-n_1}{k\epsilon_1} & \frac{k_-(R-v_F)n_1}{\epsilon_1(\epsilon_1+\lambda)} & \frac{k_-n_2}{k\epsilon_2} & \frac{k_-(R+v_F)n_2}{\epsilon_2(\epsilon_2+\lambda)}\\ \frac{-ik_+n_1}{k\epsilon_1} & \frac{-ik_+(R-v_F)n_1}{\epsilon_1(\epsilon_1+\lambda)} & \frac{ik_+n_2}{k\epsilon_2} & \frac{-ik_+(R+v_F)n_2}{\epsilon_2(\epsilon_2+\lambda)}\\ \frac{-k(R-v_F)n_1}{\epsilon_1(\epsilon_1+\lambda)} & \frac{n_1}{\epsilon_1} & \frac{k(R+v_F)n_2}{\epsilon_2(\epsilon_2+\lambda)} & \frac{n_2}{\epsilon_2}\end{pmatrix}\begin{pmatrix}b'_1\\ a'_1\\ b'_2\\ a'_2\end{pmatrix}. \tag{4.11}$$

Here we dropped the indices of k. By the same approximations, we have the form factor

$$f_1=\frac{kp}{2\epsilon_{1\mathbf{k}}\epsilon_{1\mathbf{p}}}\left[(R-v_F)^2+\left(\frac{(R-v_F)^4}{(\epsilon_{1\mathbf{k}}+\lambda)(\epsilon_{1\mathbf{p}}+\lambda)}+\frac{(\epsilon_{1\mathbf{k}}+\lambda)(\epsilon_{1\mathbf{p}}+\lambda)}{k^2p^2}\right)\left(\frac{\mathbf{k}\cdot\mathbf{p}}{2}\right)\right], \tag{4.12}$$

for band 1 and

$$f_2=\frac{kp}{2\epsilon_{2\mathbf{k}}\epsilon_{2\mathbf{p}}}\left[(R+v_F)^2+\left(\frac{(R+v_F)^4}{(\epsilon_{2\mathbf{k}}+\lambda)(\epsilon_{2\mathbf{p}}+\lambda)}+\frac{(\epsilon_{2\mathbf{k}}+\lambda)(\epsilon_{2\mathbf{p}}+\lambda)}{k^2p^2}\right)\left(\frac{\mathbf{k}\cdot\mathbf{p}}{2}\right)\right] \tag{4.13}$$

for band 2. We consider only the valence band 1 and conduction band 1 because they have the smaller band gap and larger density of states near Fermi surface. The resulting Hamiltonian with external field is,

$$H_1=\sum_{\mathbf{k}}\epsilon^v_{\mathbf{k}}a'_{1\mathbf{k}}a'^\dagger_{1\mathbf{k}}+\epsilon^c_{\mathbf{k}}b'^\dagger_{1\mathbf{k}}b'_{1\mathbf{k}}+\sum_{\mathbf{k},\mathbf{p}}V_{\mathbf{k}-\mathbf{p}}f_1(\mathbf{k},\mathbf{p})b'^\dagger_{1\mathbf{k}}a'^\dagger_{1\mathbf{p}}a'_{1\mathbf{k}}b'_{1\mathbf{p}}. \tag{4.14}$$

doi:10.6342/NTU201901151

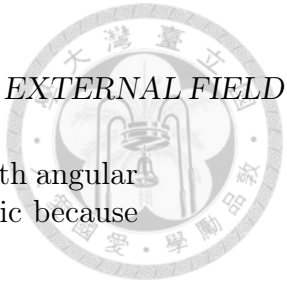

It is important to point out that the form factor contains a term with angular dependence. The solutions of the gap equations can be anisotropic because of its presence.

doi:10.6342/NTU201901151

doi:10.6342/NTU201901151

Chapter 5

The Gap Equation and Its Solution

We derive the gap equation analogous to BCS theory in superconductors. It turns out that there are three types of solutions distinguished by the symmetric property in k-space. We showed the lowest energy state is the mixture of symmetric and anti-symmetric solutions.

5.1 Gap equation

When electron-hole pairs form in a system, it is natural to consider the commutation relation between pairs. The excitons behave like bosons as the mean distance between two excitons is much larger than the extension of excitons [32]. In the condensed phase, on the other hand, electrons and holes are to be treated separately as fermions and BCS states prevails. The BCS ground state [34] is

$$|\Psi_{\mathrm{BCS}}\rangle = \prod_{\mathbf{k}} (u_{\mathbf{k}} + v_{\mathbf{k}} c^{\dagger}_{\mathbf{k}} c^{\dagger}_{-\mathbf{k}}) \, |\Phi\rangle \,, \tag{5.1}$$

where $c^{\dagger}_{\mathbf{k}} c^{\dagger}_{-\mathbf{k}}$ is a Cooper pair operator which create an electron pair in momentum space near Fermi surface.

Let $|\Phi\rangle$ be the state with full valence band and empty conduction band and replace e-e pair with e-h pair in the ground state [35]. The wave function of exciton condensate is

$$|\Psi_{\mathrm{ex}}\rangle = \prod_{\mathbf{k}} (u^{*}_{\mathbf{k}} - v^{*}_{\mathbf{k}} b^{\dagger}_{\mathbf{k}} a_{\mathbf{k}}) \, |\Phi\rangle \,. \tag{5.2}$$

where $b^{\dagger}_{\mathbf{k}} a_{\mathbf{k}}$ is the creation operator of e-h pair. It is also instructive to see the form of quasi-particle excitation. For excitons, excitations can be defined

doi:10.6342/NTU201901151

as $\alpha_{\mathbf{k}} = u_{\mathbf{k}}a_{\mathbf{k}} - v_{\mathbf{k}}b_{\mathbf{k}}$, and $\beta_{\mathbf{k}} = v^*_{\mathbf{k}}a_{\mathbf{k}} + u^*_{\mathbf{k}}b_{\mathbf{k}}$. Comparing with the BCS theory, we can easily find the analogous Bogoliubov quasi-particle operators $\gamma_{\mathbf{k}} = u_{\mathbf{k}}c_{\mathbf{k}} - v_{\mathbf{k}}c^\dagger_{-\mathbf{k}}$, $\gamma_{-\mathbf{k}} = u_{\mathbf{k}}c_{-\mathbf{k}} + v_{\mathbf{k}}c^\dagger_{\mathbf{k}}$. The coefficient $u_{\mathbf{k}}$ and $v_{\mathbf{k}}$ satisfy the condition $|u_{\mathbf{k}}|^2 + |v_{\mathbf{k}}|^2 = 1$ in both exciton condensation and superconductor cases. Similar to the BCS theory, we minimize the total energy with respect to $u_{\mathbf{k}}$ and $v_{\mathbf{k}}$ and the results are

$$u_{\mathbf{k}} = \left[\frac{1}{2}\left(1 + \frac{\xi_{\mathbf{k}}}{E_{\mathbf{k}}}\right)\right]^{1/2}, \qquad v_{\mathbf{k}} = \left[\frac{1}{2}\left(1 - \frac{\xi_{\mathbf{k}}}{E_{\mathbf{k}}}\right)\right]^{1/2}, \tag{5.3}$$

where

$$\xi_{\mathbf{k}} = (\epsilon^c_{\mathbf{k}} - \epsilon^v_{\mathbf{k}})/2, \qquad E^2_{\mathbf{k}} = \xi^2_{\mathbf{k}} + \Delta^2_{\mathbf{k}}. \tag{5.4}$$

Using the effective Coulomb potential given by Hamiltonian (4.9), the self consistent gap equation at zero temperature can be determined as

$$\Delta_{\mathbf{k}} = \sum_{\mathbf{p}} f_i(\mathbf{k},\mathbf{p}) V_{\mathbf{k}-\mathbf{p}} \frac{\Delta_{\mathbf{p}}}{2\sqrt{\xi^2_{\mathbf{p}} + |\Delta_{\mathbf{p}}|^2}}, \tag{5.5}$$

where $i = 0, 1$ are for the case without or with external field.

5.2 Solution of gap equation

We have derived the gap equation in the last subsection. More explicitly, we have an integral equation as

$$\Delta(k_x, k_y) = \frac{1}{(2\pi)^2}\int_{B.Z.} f_i(\mathbf{k},\mathbf{p}) V_{\mathbf{k}-\mathbf{p}} \frac{\Delta(p_x,p_y)}{2\sqrt{\xi^2_{\mathbf{k}} + \Delta^2(p_x,p_y)}} dp_x dp_y. \tag{5.6}$$

The domain of integration is over the first Brillouin zone instead of an artificial cutoff introduced in the work of Kozlov and Maksimov [14]. In their work, case B of part 3, they assumed the gap remains a constant value $\Delta(0)$ for $p < p_1$, the cutoff. They also argued that $\Delta(\mathbf{p})$ decreased rapidly as $p > p_1$. Determining of p_1 is based on dispersion relation which is a relatively simple band structure $\epsilon(p) = p^2/2$. Let $\Delta(0) = p_1^2/2$ and solving for p_1 leads to $p_1 = \sqrt{2\Delta(0)}$. There is no reason to set any cut-off momentum here since the dispersion relation here is close to being linear. The gap Δ does not behave as Kozlov and Masksimov [14] had assumed. It will be even clearer in the solution level which we will see later.

doi:10.6342/NTU201901151

5.2.1 Numerical solutions

We solve the integral equation with the following recipe. First we give a specific value k_{yi} and a trial Δ and evaluate the integration. This will give a rough curve of $\Delta(k_x)$ versus k_x, called $\Delta_0(k_x)$. Second we feed the $\Delta_0(k_x)$ back into integration and repeat the processes. We can start with trial wave functions with different symmetries in region $k_x = [\frac{-\pi}{a}, \frac{\pi}{a}]$, then do the iteration. Finally the output function will converge to a form with enough accuracy, which is set as 10^{-3} in this work. We apply the same process for the case with external field. The region of $k_y = [-\frac{\pi}{a}, \frac{\pi}{a}]$ is divided by 33 intervals. We did the iteration to get $\Delta(k_x)$ for every k_{yi}. The grids are 33×33 in the first Brillouin zone. Momentum k_x and k_y are centered at $\mathbf{k} = 0$ which is the **K** point of germanene and silicene.

Parameters are given in [27] for germanene. The length is measured for lattice constant $a \approx 4$Å. Energy is in unit of Fermi velocity times k, where $v_F \approx 4.57 \times 10^{-5}$ cm/s. λ, half of band energy gap, is 46meV and internal Rashba interaction r is 10.7meV for gemanene. By Ref. [31], in the case without external field $x_M = 25E_g$ thus $\alpha^0_{2D} \approx \frac{e^2}{2\pi E_g}(\frac{1}{1} - \frac{1}{26}) \times 2 = 48.07$Å, where the factor of 2 is the number of degenarate bands, see FIG. 3.1(a). As for the case with external field $\alpha^1_{2D} \approx \frac{e^2}{2\pi E_g}[(\frac{1}{1} - \frac{1}{7.25}) + 1] = 46.55$Å, where the first term comes form band 1 and the second term comes from band 2, see FIG. 3.1(b). Examples of symmetric and anti-symmetric iterations are shown in FIG. 5.1. The red curve is the initial one and the black curve is the final result.

For a comprehensive consideration, the ground state can be either purely symmetric or anti-symmetric but also the linear combination of them. In order to give a complete physical pictures, we give three contour plots of gap functions in the first Brillouin zone in FIG. 5.2. and FIG. 5.3. Apparently, the symmetric solution is nodeless. The antisymmetric one has a node line. Interestingly, the gap function of the mixed solution almost vanishes in left half plane. It is equally possible that its magnitude is vanishingly small in either upper or lower half plane.

Now the question occurs: which solution gives the lowest energy? To answer this, we have calculated the energy of each solution. The wave function of exciton condensed state is similar to BCS theory. The form of energy can be deduced from the BCS theory [36] which reads

$$E = \sum_{\mathbf{k}} \left[\epsilon_{\mathbf{k}}(1 + 2x_{\mathbf{k}}) - (\frac{1}{4} - x^2_{\mathbf{k}})^{1/2} \Delta_{\mathbf{k}} \right], \tag{5.7}$$

doi:10.6342/NTU201901151

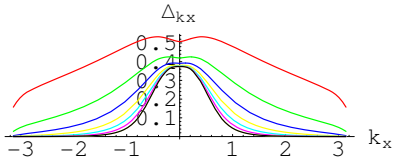

(a) symmetric solution

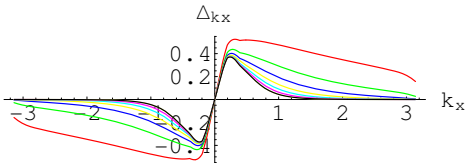

(b) anti-symmetric solution

Figure 5.1: For $k_y = 0.2$, the iteration processes (red curve $\rightarrow$ black curve) of (a) symmetric and (b) anti-symmetric solution of $\Delta(k_x)$ *without eternal field*.

where $x_{\mathbf{k}} = \pm\frac{\epsilon_{\mathbf{k}}}{2\sqrt{\epsilon_{\mathbf{k}}^2+\Delta_{\mathbf{k}}^2}}$. We insert $\Delta_{\mathbf{k}}$ obtained from the integral equation into Eq. (5.7). In the three cases, the anti-symmetric $\Delta_{\mathbf{k}}$ state has the highest energy thus it cannot be the condensation state. Another possible form of solution, $\Delta_0(k_x + ik_y)$, which is common in considering p-wave superconductors is also considered. This solution gives energy comparable to that of the antisymmetric state. Thus it cannot be the condensation either. We found the energy of mixed solution is slightly lower than the symmetric one. Defining a parameter $\eta \equiv (E^s - E^m)/E^m$, where superscript s and m stand for symmetric and mixed, respectively. $\eta^{int} \approx 0.006$ when only intrinsic Rashba interaction is considered. However, $\eta^{ex} \approx 0.03$ as an external electrical field $R = 1.2v_F$ is applied. We can see the energy difference is not significant when there is no external field. It is more advantageous to the mixed wave state by applying electric field. In short, the mixed state is the ground state of exciton condensation under external electrical field.

We plot the diagram of Δ versus band gap ($E_g = 2\lambda$) of semiconductor, see FIG. 5.4. The red curve is the case without external field while the black one is the case with external field. The bandwidth of germanene is also pointed out in FIG. 5.4. The regions under the curves are where the condensation states are stable. This diagram shows that the exciton condensation state is the ground state of the system thus the e-h pairs can, in principle, survive for a long time. As we estimated before, $\alpha_{2D}^0 > \alpha_{2D}^1$, thus the 2D Coulomb potential with external field is stronger. This leads to a larger Δ for germanene.

doi:10.6342/NTU201901151

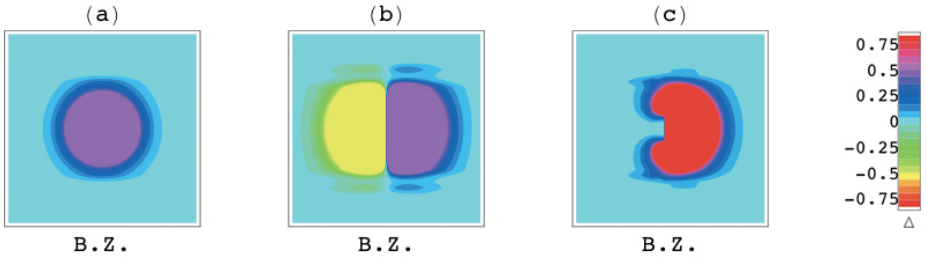

Figure 5.2: The contours of symmetric (a) symmetric, (b) anti-symmetric, and (c) mixed solutions *without external field* for germanene.

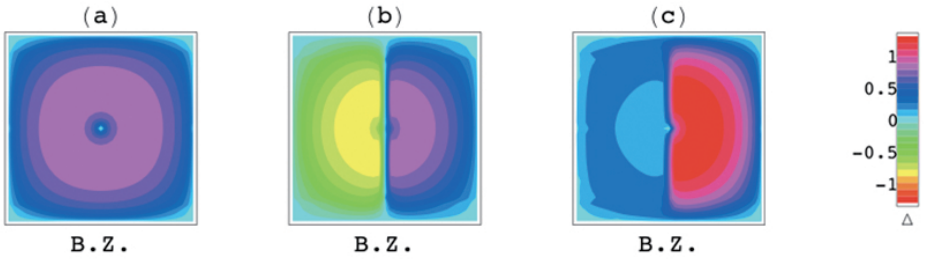

Figure 5.3: The contours of (a) symmetric, (b) anti-symmetric, and (c) mixed solutions *with external field* $R = 1.2v_F$ for germanene.

5.2.2 Approximate form of solutions

To give a clearer picture, we try an approximation solution of $\Delta(\mathbf{k}) \approx \Delta_0(k) + \Delta_1(k)\cos\theta_k$ where $\theta_k = \tan^{-1}(k_y/k_x)$. This can show us the amplitudes of the s-wave and p-wave in the mixed state. Then the integral equation in polar coordinate is

$$\Delta_0(k)+\Delta_1(k)\cos\theta_k = \frac{1}{\pi^3}\int_0^{2\pi}\int_0^{\pi} V(k,\theta_k;p,\theta_p)f_1(k,\theta_k;p,\theta_p)K(p,\theta_p)pdpd\theta_p, \tag{5.8}$$

where the integration kernel $K(p,\theta_p) = \frac{\Delta_0(p)+\Delta_1(p)\cos\theta_p}{2\sqrt{\epsilon_p^2+(\Delta_0(p)+\Delta_1(p)\cos\theta_p)^2}}$. Coulomb potential V and form factor f_1 can be found in Eq. (4.3) and Eq. (4.12), respectively. Our first equation is given by integrating θ_k over 0 to 2π and solving Δ_0 for a given k. More specifically,

$$\Delta_0 = \frac{1}{\pi^3(2\pi)}\int_0^{2\pi}\int_0^{2\pi}\int_0^{\pi} V(k,\theta_k;p,\theta_p)f_1(k,\theta_k;p,\theta_p)K(p,\theta_p)pdpd\theta_p d\theta_k \tag{5.9}$$

doi:10.6342/NTU201901151

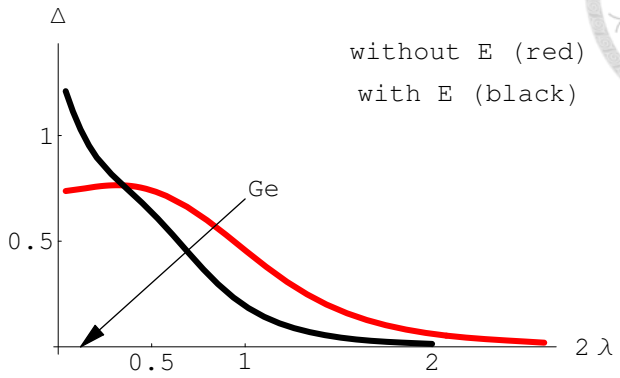

Figure 5.4: The diagram of Δ at $(k_x, k_y) = (0.2, 0)$ for different semiconductor band gap 2λ.

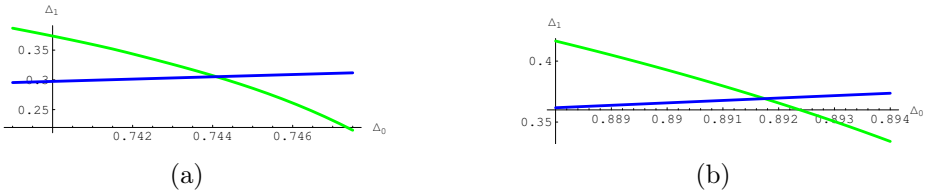

(a) (b)

Figure 5.5: The green curve is plotted with Eq. (5.9) and blue curve is plotted with Eq. (5.10). Intersection of two curves is the solution of (Δ_0, Δ_1). (a) $(k_x, k_y) = (0.35, 0.2)$ (b) $(k_x, k_y) = (0.8, 0.6)$

Then we multiply $\cos\theta_k$ on both side of Eq. (5.8) and perform an integration $\frac{1}{2\pi}\int d\theta_k$, which leads to

$$\Delta_1 = \frac{2}{\pi^3(2\pi)}\int_0^{2\pi}\int_0^{2\pi}\int_0^{\pi} V(k,\theta_k;p,\theta_p) f_1(k,\theta_k;p,\theta_p) K(p,\theta_p)\cos\theta_k p dp d\theta_p d\theta_k. \tag{5.10}$$

Now we have two coupled equations for Δ_0 and Δ_1. For a given set of (k_x, k_y), there will be two curves from Eq. (5.9) and Eq. (5.10). The intersection is the solution. For example in FIG. 5.5(a), $(k_x, k_y) = (0.35, 0.2)$, the numerical results of Eq. (5.9) (green) and Eq. (5.10) (blue) are shown. These two curves intersect at point $(\Delta_0, \Delta_1) = (0.744, 0.305)$. Our approximate gap $\Delta_0 + \Delta_1\cos\theta_k = 0.744 + 0.305\cos(\tan^{-1}\frac{0.2}{0.35}) \approx 1.01$. This should be compared with the iteration result for $(k_x, k_y) = (0.35, 0.2)$ of mixed state solution in FIG.5.6 (purple), where the numerical result is $\Delta \approx 1.05$, the accuracy is reasonable and the difference comes from the integration boundary [37]. Another example is in FIG. 5.5(b), $(k_x, k_y) = (0.8, 0.6)$ and solved $(\Delta_0, \Delta_1) = (0.892, 0.37)$. $\Delta_0 + \Delta_1\cos\theta_k = 0.892 + 0.37\cos(\tan^{-1}\frac{0.6}{0.8}) \approx 1.19$ which is also

doi:10.6342/NTU201901151

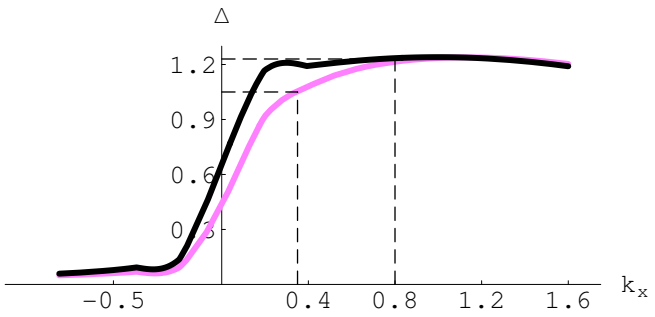

Figure 5.6: Numerical mixed state solution of Δ as $k_y = 0.2$ (purple) and $k_y = 0.6$ (black) for germanene.

close to the numerical result $\Delta \approx 1.23$, see FIG. 5.6 (black). The amplitude of p-wave type (anti-symmetric) solution if exists is usually much smaller than that of the s-wave (symmetric) solution in superconductors. Here the magnitude of Δ_0 and Δ_1 are comparable in this 2D system with external field. Hence, the mixed state has significant symmetric and antisymmetric parts.

doi:10.6342/NTU201901151

doi:10.6342/NTU201901151

Chapter 6

Proposed Experiment

Exciton condensate can be observed in various ways. The most commonly used is the optical method. L.V. Butov and A.I. Filin [38] used photoluminescence to investigate the exciton condensate in quantum well systems. They found superradiance due to the coherence of the condensed exciton states in contrast to normal excitons. One can also observe the condensate by interference of lights emitted from an array of beads of condensate [39] or two traps connected by Josephson tunneling of coherent excitons [12].

The transport measurement can also provide evidence of exciton condensate. Although exciton current is not charged, one can turn to thermal conductivity for the onset of condensation. Rontani and Sham [12] applied Bogoliubov-de Gennes equation [40] to a semimetal-semiconductor structure and calculated the transmission coefficient. They found that the thermal conductivity as a function of temperature exhibits activation behavior with the activation energy being the energy gap of the exciton condensate on the semimetal side. Applying their theory to our system, we found that the s-wave condensate should also have this property. On the other hand, the mixed state does not have any activation energy because its energy gap is vanishingly small for $k_x < 0$.

The mixed state we found has other interesting properties. One of them is the existence of midgap state in a sNp structure in which a semimetal layer in normal state is sandwiched between two semimetal layers, one in s-wave state and the other in mixed state. Therefore, in subsection A we show that the excitons in germanene or silicene are a mixture of bright and dark excitons and hence, can be detected with optical methods. In subsection B we derived the wave function and energy of the midgap states. Thus, in addition to the experimental methods of superradiance and optical interference mentioned above, our result can also be verified by looking for the midgap states.

doi:10.6342/NTU201901151

6.1 Luminal properties of exciton condensation

In the previous work of Ref. [41], Combescot *et al.* provided a rule of Bose-Einstein condensation in semiconductors. They first define bright and dark excitons by their optical properties. *Bright* excitons have total angular momentum 1 so they may be coupled with photons while *dark* excitons with total angular momentum 2 cannot. The configuration of our 2D system is more complex than those discussed by M. Combescot *et al.* [41]. The spin 3/2 and 1/2 states are mixed in both conduction and valence band. Hence it needs a finer treatment. Consider the case without external field.

Let's look at the coefficients in (3.6). Since $r \ll v_F$, functions with coefficients B_k and C_k can be neglected. Coefficient A_k approaches zero as $k \to 0$ and increases monotonically to 1 for increasing k and has to be considered. Also, the s-orbital doesn't provide any effect as discussed by Combescot *et al.* [41]. We consider the functions of $|\phi_1\rangle$ and $|\phi_4\rangle$ as

$$\begin{aligned}\left|\phi_{1\uparrow(\downarrow)}\right\rangle &\sim \left[u_{11}\left|p_z^A\right\rangle + \frac{u_{31}}{\sqrt{2}}(\left|p_x^B\right\rangle - i\left|p_y^B\right\rangle)\right] \otimes |\uparrow\rangle\,(|\downarrow\rangle),\\ \left|\phi_{4\uparrow(\downarrow)}\right\rangle &\sim \left[u_{11}\left|p_z^B\right\rangle - \frac{u_{31}}{\sqrt{2}}(\left|p_x^A\right\rangle + i\left|p_y^A\right\rangle)\right] \otimes |\uparrow\rangle\,(|\downarrow\rangle),\end{aligned} \tag{6.1}$$

The simplified compositions of conduction and valence bands are

$$\begin{aligned} b_1 &\sim A_k\,|\phi_{1\uparrow}\rangle + |\phi_{4\uparrow}\rangle \qquad & a_1 &\sim -A_k\,|\phi_{1\downarrow}\rangle + |\phi_{4\downarrow}\rangle\,,\\ b_2 &\sim |\phi_{1\downarrow}\rangle + A_k^*\,|\phi_{4\downarrow}\rangle & a_2 &\sim |\phi_{1\uparrow}\rangle - A_k^*\,|\phi_{4\uparrow}\rangle\,.\end{aligned} \tag{6.2}$$

We then relabel the $|p\rangle \otimes |\sigma\rangle$ states as $|l, l_z\rangle\,|s, s_z\rangle$. For example, $|\phi_{1\uparrow}\rangle$ in (6.1) can be written as

$$\begin{aligned}|\phi_{1\uparrow}\rangle &\sim u_{11}\,|1,0\rangle\left|\tfrac{1}{2},\tfrac{1}{2}\right\rangle_A + u_{31}\,|1,-1\rangle\left|\tfrac{1}{2},\tfrac{1}{2}\right\rangle_B\\ &= u_{11}\left(\sqrt{\tfrac{2}{3}}\left|\tfrac{3}{2},\tfrac{1}{2}\right\rangle_A - \sqrt{\tfrac{1}{3}}\left|\tfrac{1}{2},\tfrac{1}{2}\right\rangle_A\right) + u_{31}\left(\sqrt{\tfrac{1}{3}}\left|\tfrac{3}{2},\tfrac{-1}{2}\right\rangle_B - \sqrt{\tfrac{2}{3}}\left|\tfrac{1}{2},\tfrac{-1}{2}\right\rangle_B\right),\end{aligned} \tag{6.3}$$

where $|l, l_z\rangle\,|s, s_z\rangle$ is written as linear combinations of $|j, m\rangle$ in the second line. j and m are total angular momentum and azimuthal angular momentum numbers, respectively. Consider the pairing of channel 1 in (6.2), this gives the configuration

$$\begin{aligned}&(1 + A_k)u_{11}\left[\sqrt{\tfrac{2}{3}}\left|\tfrac{3}{2},\tfrac{1}{2}\right\rangle_A - \sqrt{\tfrac{1}{3}}\left|\tfrac{1}{2},\tfrac{1}{2}\right\rangle_A\right]\\ &+ u_{31}\left[A_k\sqrt{\tfrac{1}{3}}\left|\tfrac{3}{2},\tfrac{-1}{2}\right\rangle_B - A_k\sqrt{\tfrac{2}{3}}\left|\tfrac{1}{2},\tfrac{-1}{2}\right\rangle_B - \left|\tfrac{3}{2},\tfrac{3}{2}\right\rangle_B\right]\end{aligned} \tag{6.4}$$

doi:10.6342/NTU201901151

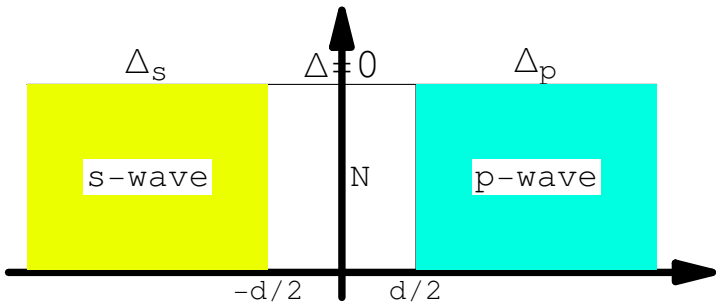

Figure 6.1: sNp structure consisting of a normal slab in the yz plane having a thickness d between semiconductors with s-wave and p-wave.

for conduction band, and

$$\begin{aligned}&(1-A_k)u_{11}\left[\sqrt{\tfrac{2}{3}}\left|\tfrac{3}{2},\tfrac{-1}{2}\right\rangle_A-\sqrt{\tfrac{1}{3}}\left|\tfrac{1}{2},\tfrac{-1}{2}\right\rangle_A\right]\\&-u_{31}\left[A_k\sqrt{\tfrac{1}{3}}\left|\tfrac{3}{2},\tfrac{-3}{2}\right\rangle_B+\sqrt{\tfrac{1}{3}}\left|\tfrac{3}{2},\tfrac{1}{2}\right\rangle_B+\sqrt{\tfrac{2}{3}}\left|\tfrac{1}{2},\tfrac{1}{2}\right\rangle_B\right]\end{aligned}\tag{6.5}$$

for valance band.

The overlap between distinct sublattices is negligible. Taking sublattice B as an example, $\left|\frac{3}{2},-\frac{3}{2}\right\rangle$ in Eq. (6.5) is a valence electron with orbital state $l_z=-1$ and spin state $\sigma=-\frac{1}{2}$, which can also be viewed as a spin $\frac{3}{2}$ hole. It may pair with other states on B sublattice. A bright exciton forms as it pairs with $\left|\frac{3}{2},-\frac{1}{2}\right\rangle$ in Eq. (6.4), *i.e.* state with $l_z=1$ and $\sigma=-\frac{1}{2}$ whilst pairing with $\left|\frac{3}{2},\frac{3}{2}\right\rangle$ gives rise a dark exciton [41]. We show that the bright and dark excitons are mixed naturally due to SOC. Hence, in each case, the exciton condensate can be observed with optical methods. Similar conclusion can be applied to condensate with external electric field. This property makes 2D semiconductors being good candidates of revealing exciton condensation.

6.2 Midgap states of exciton condensation

We discuss another possible way to probe the existence of exciton condensation by analyzing the midgap state. Analogous to the superconductor-normal metal-superconductor system, in FIG. 6.1, we set up an sNp sandwich system where s, N, and p represent the symmetric condensation state, semimetal, and mixed condensation state, respectively. The s-wave condensation can come from any semiconductors with desired property and the p-wave condensation denotes germanene. The midgap state resides in the N layer and

doi:10.6342/NTU201901151

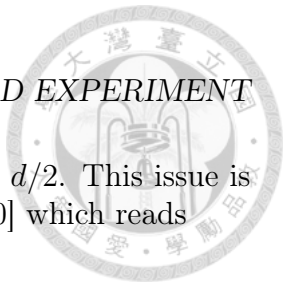

its wave function decreases exponentially in regions $|x| > d/2$. This issue is studied by solving the Bogoliubov-de Gennes equation [40] which reads

$$\begin{aligned} -i\hbar v_F \frac{d}{dx} u(x) + \Delta(\mathbf{k}, \mathbf{x}) v(x) &= \epsilon u(x) \\ \Delta(\mathbf{k}, \mathbf{x}) u(x) + i\hbar v_F \frac{d}{dx} v(x) &= \epsilon v(x), \end{aligned} \tag{6.6}$$

with

$$\begin{aligned} \Delta(\mathbf{k}, \mathbf{x}) &= \Delta_s, \qquad x < -d/2 \\ &= 0, \qquad -d/2 < x < d/2 \\ &= \Delta_p, \qquad x > d/2. \end{aligned}$$

In the case of $k_x > 0$ and assuming $\epsilon < |\Delta|$ we have the solution for region $-d/2 < x < d/2$ ($\Delta = 0$) as

$$\begin{pmatrix} u(x) \\ v(x) \end{pmatrix} = A \left[e^{i\lambda_N x} \begin{pmatrix} 1 \\ 0 \end{pmatrix} + a e^{i\lambda_N x} \begin{pmatrix} 0 \\ 1 \end{pmatrix} \right], \tag{6.7}$$

where $\lambda_N = \epsilon(\hbar v_F)^{-1}$. The solution for two sides are

$$\begin{pmatrix} u(x) \\ v(x) \end{pmatrix}_P = c e^{-\lambda_p x} \begin{pmatrix} \tilde{u}_p \\ \tilde{v}_p \end{pmatrix} \tag{6.8}$$

and

$$\begin{pmatrix} u(x) \\ v(x) \end{pmatrix}_S = c' e^{-\lambda_s x} \begin{pmatrix} \tilde{u}_s \\ \tilde{v}_s \end{pmatrix}, \tag{6.9}$$

where $\lambda_{s(p)} = \sqrt{|\Delta_{s(p)}|^2 - \epsilon^2}/\hbar v_F$, $\tilde{u}_{s(p)} = \frac{1}{\sqrt{2}}(1 + i\sqrt{|\Delta_{s(p)}|^2 - \epsilon^2}/\epsilon)^{1/2}$, and $\tilde{v}_{s(p)} = \frac{1}{\sqrt{2}}(1 - i\sqrt{|\Delta_{s(p)}|^2 - \epsilon^2}/\epsilon)^{1/2}$. Continuity of wave function at two interfaces $x = \pm d/2$ gives us

$$a e^{-i\lambda_N d} = \tilde{v_p}/\tilde{u_p}, \qquad a e^{i\lambda_N d} = \tilde{u_s}/\tilde{v_s}.$$

Thus we have the bound state condition

$$e^{2i\lambda_N d} = \frac{\tilde{u_p}}{\tilde{v_p}} \frac{\tilde{u_s}}{\tilde{v_s}}. \tag{6.10}$$

This condition is similar to that of the case in d-wave superconductors [42]. For definiteness, define $\sin\alpha = \epsilon/|\Delta_s|$ and $\sin\beta = \epsilon/|\Delta_p|$ with the domain of α and β being $[-\frac{\pi}{2}, \frac{\pi}{2}]$. Inserting the explicit expression of $\tilde{u}$ and $\tilde{v}$, we have

$$e^{2i\lambda_N d} = \left[\frac{(\sin\alpha + i\cos\alpha)(\sin\beta + i\cos\beta)}{(\sin\alpha - i\cos\alpha)(\sin\beta - i\cos\beta)} \right]^{1/2},$$

doi:10.6342/NTU201901151

(a) (b)

Figure 6.2: The midgap state energy versus k_x for (a) sNp and (b) sNs structures.

which leads to

$$\epsilon = \hbar\omega_F \left[-\frac{1}{2}\left(\sin^{-1}\frac{\epsilon}{|\Delta_s|} + \sin^{-1}\frac{\epsilon}{|\Delta_p|} \right) + \pi(l+\frac{1}{2}) \right], \tag{6.11}$$

where l is an integer and $\omega_F \equiv d(\hbar v_F)^{-1}$ is the inverse of time needed for a particle moves from one end of N region to the other. We can obtain the solution for $k_x < 0$ by similar calculation which reads,

$$\epsilon = \hbar\omega_F \left[-\frac{1}{2}\left(\sin^{-1}\frac{\epsilon}{|\Delta_s|} + \sin^{-1}\frac{\epsilon}{|\Delta_p|} \right) + \pi(l-\frac{1}{2}) \right]. \tag{6.12}$$

On the other hand, for the sNs structure, binding energy ϵ' can be derived by a similar way which reads

$$\epsilon' = \hbar\omega_F \left[-\sin^{-1}\frac{\epsilon'}{|\Delta_s|} + \pi(l \pm \frac{1}{2}) \right]. \tag{6.13}$$

In FIG. 6.2, we sketch the energy solution ϵ and ϵ' versus momentum k_x for a given k_{y0} in the case with external field.

The midgap state energy for sNp structure becomes vanishingly small for $k_x < 0$ while that of sNs structure is finite in the entire range of k_x. This is because $|\Delta_p|$ approaches zero when k_x become more negative (FIG. 5.6). Since $|\epsilon| < |\Delta_p|$, $|\epsilon|$ is also small whilst ϵ' in sNs structure has to be finite due to the term $l \pm \frac{1}{2}$ in Eq. (6.13). For $|\Delta_p|$ approaching zero, Eq. (6.11) can be simplified to $-\sin^{-1}\frac{\epsilon}{|\Delta_p|} \pm \pi = 0$. The plus sign ($l = 0$) gives a solution $\epsilon = 0^+$ while the minus sign ($l = -1$) gives a solution $\epsilon = 0^-$. A similar argument can be made for Eq. (6.12) which gives $\epsilon = 0^-$ as ($l = 0$) and $\epsilon = 0^+$ for $l = 1$, respectively. In both cases, the magnitude of ϵ is closed to that of $|\Delta_p|$. There is no solution in region $l > 1$ or $l \leq -1$ for which the equation is positive definite and negative definite, respectively. On the other hand, ϵ' in Eq. (6.13) remains finite as $k_x < 0$.

Unlike that in superconductors, the electron-hole paired quasiparticle is charge neutral. We cannot measure the midgap states via conductivity or

doi:10.6342/NTU201901151

any electromagnetic experiments. The midgap states should be measured by any technique which is sensitive to the energy dependence of the density of states such as thermal conductivity. Though in FIG. 6.2(a) the energy of the mid-gap state vanishes in the $-k_x$ region, it is equally likely that it vanishes in the $-k_y$ region. In sNp structure, the interface can be perpendicular to either x- or y-direction. The zero-energy midgap states should exist in one of two cases. If thermal conductance measurements are taken at low temperature, the case without zero-energy midgap state will show activation behavior and the other with zero-energy mid-gap state will exhibit finite thermal conductance.

doi:10.6342/NTU201901151

Chapter 7

Introduction of Magnon Condensate in CuO

Materials that exhibit several primary ferroic order parameters are called multiferroics. They include, for example, magnetic orders, ferroelectricity, ferroelasticity, etc. Among them, magnetic orders and ferroelectricity interest physicist mainly because of the magnetoelectric effect. Multiferroics often are transition metal oxides such as $TbMnO_3, HoMn_2O_5, LuFe_2O_4$ and what we will discuss here, cupric oxide (CuO). For the potential of applications, it is desirable to have high critical temperature and strong electric-magnetic coupling. Cupric oxide is a good candidate.

The study of CuO started quite early. The lattice structure was analyzed by Asbrink and Norrby [43]. In the late 80's and early 90's more experimental results were reported [44, 45, 46]. Their works are the measurement of susceptibility and the study of magnetic structure via neutron scattering. Two transition temperatures had been found, $T_{N_1} = 213$K is the phase transition temperature from colinear spin to spiral spin phase whist $T_{N_2} = 230$K is the transition temperature from spiral spin phase to paramagnetic phase. In the early 2000, CuO again attracted people's attention after the discovery of multiferroicity of CuO by T. Kimura *et al.* [47]. The spiral spin configuration and hence, the multiferroic phase occurs in the temperature range of 20K.

The theoretical research is an interesting topic even nowadays. Filippetti and Fiorentini [48] use first-principle self-interaction-free-density-functional approach to study the magnetic ordering in CuO. Their conclusion is that low-dimensional approach is not enough for the ground state of CuO. Three dimensional exchange interactions are necessary. Giovannetti *et al.* [49] focused on the multiferroics of CuO. Guang Jin *et al.* [50] discussed the origin of multiferroicity of CuO. Although the multiferroics is not the subject of this

doi:10.6342/NTU201901151

paper, their results gave a more clear picture of the strength of exchange. A detailed discussion of the phases of CuO can be found in the paper by R. Villarreal *et al.* [51]. Pierre Toledano *et al.* [52] achieved progresses, especially they gave a possible configuration of spins. We will eleborate their work later. As shown in the first-principle calculations, CuO has very complex spin couplings. Ref. [48] introduced five coupling constants in order to reach realistic spin configuration and electronic structure. Here, we choose the analytical calculation which is complementary to numerical analysis and can provide additional physical insight. The computation method we use is the Schwinger boson mean-field theory (SBMFT) [53]. It is able to handle complicated exchange interaction. It has advantage over the well-known Holstein-Primakoff transformation, in that we can account for chosen order parameters and the effect of their interplay.

We applied SBMFT to spiral spin configuration and introduced two order parameters. By diagonalizing the Hamiltonian we found excitation energy and Bose-Einstein condensations at finite momenta. When the approach was applied to CuO, we were able to obtain magnetic magnetic susceptibility measured in Ref. [45]. The concept of entropy is used in the work of Guang Jin *et al.* [50] to discuss the origin of ferroeletricity. According to their calculation, the effect of entropy in clear is a large enough lattice. We also demonstrate that the entropy plays a crucial role in commensurate-incommensurate $(c - ic)$ phase transition. Our model offers a more intuitive picture in dealing with entropy.

Chapter 7-10 are organized as follow. Chapter 7 is the introduction of magnons in CuO. In Ch.8, we generalized spin rotation idea and introduced Schwinger boson (SB) method. Ch.9 is the application of the SB method to CuO, including the construction of spin configurations, the calculation of BEC momentum, and the magnetic susceptibility as well. We give a scenario of commensurate-incommensurate phase transition in Ch.10.

doi:10.6342/NTU201901151

Chapter 8

Formulation of SBMFT

8.1 Spin rotation

We consider a system of interacting spins. The spins form a lattice with basis and there can be more than one spin in the basis. Our spin interaction system is described by the quantum Heisenberg model

$$H = \sum_{<ni,mj>} J_{ni,mj}\mathbf{S}_{ni} \cdot \mathbf{S}_{mj} + \mathbf{D}_{ni,mj} \cdot (\mathbf{S}_{ni} \times \mathbf{S}_{mj}). \tag{8.1}$$

The indices n and m indicate the position of unit cells whose origins are at $\mathbf{R}_n$ and $\mathbf{R}_m$, respectively. i and j label the atoms in a cell. The magnitude of interacting spin pairs is described by $J_{ni,mj}$, and the sign of $J_{ni,mj}$ indicates the direction preference: positive (negative) $J_{ni,mj}$ for antiferromagnetic (ferromagnetic) coupling. The second term is the DM interaction and we let $\mathbf{D}_{ni,mj} = D\epsilon_{ni,mj}\hat{\mathbf{y}}$. Notation $\epsilon_{ni,mj}$ is a sign tensor which equals to 1 as $i < j$ and -1 otherwise. We take the DM interaction of CuO to be along the direction of spiral axis because this is lowest energy state. The DM interaction here is one kind of anisotropy and one can consider other kinds of anisotropic interactions as well, if necessary. An additional anisotropic exchange coupling such as $KS_i^y S_j^y$ has similar effect.

Since the Hamiltonian can contain quite a few exchange coupling constants, the spin configuration can be complicated, e.g. ferromagnetic state, Neel states, canted spin state and spiral spin state. One way to treat these situations is to have local coordinates. The spin orientations vary from site to site. However, we can assign the $z-$axis in each local coordinate to be the preferred direction of the local spins. This way, the development can be made clearer. The price to pay is that one have to deal with the relative orientation between local coordinates. This method can be applied to Neel state, spiral states and canted spins if sublattices are introduced.

doi:10.6342/NTU201901151

Consider the i-th spin operator in the n-th unit cell $\mathbf{S}_{ni}$. It is rotated about y-axis which is the spiral axis by an angle $\mathbf{q}\cdot\boldsymbol{\alpha}_{ni}$ with the operator $U_{ni}=\exp(-i\mathbf{q}\cdot\mathbf{R}_{ni}S^y_{ni})$, where $\mathbf{q}$ is the magnetic modulation vector which can be identified by experiments such as neutron scattering. The rotated Hamiltonian is

$$H'=UHU^\dagger=\sum J_{ni,mj}\,\mathbf{S}'_{ni}\cdot\mathbf{S}'_{mj}+\mathbf{D}_{ni,mj}\cdot(\mathbf{S}'_{ni}\times\mathbf{S}'_{mj}),$$

where

$$\mathbf{S}'_{\mathbf{r}}=U_{\mathbf{r}}\mathbf{S}_{\mathbf{r}}U^\dagger_{\mathbf{r}}=\widehat{R}(\mathbf{q}\cdot\mathbf{r})\mathbf{S}_{\mathbf{r}},$$

and $U=\Pi U_{n.i}$. Here $\widehat{R}(\mathbf{q}\cdot\mathbf{r})$ is a SO(3) operator. In this circumstance, the spiral spin state becomes purely ferromagnetic. Replacing the position vector $\mathbf{r}$ by $\boldsymbol{\alpha}_{ni,mj}\equiv\mathbf{R}_{ni}-\mathbf{R}_{mj}$, the relative position vector of two atoms, the expression of the inner product of spins after rotation leads to

$$\mathbf{S}'_{ni}\cdot\mathbf{S}'_{mj}=(S^x_{ni}S^y_{ni}S^z_{ni})\begin{pmatrix}\cos(\mathbf{q}\cdot\boldsymbol{\alpha}_{ni,mj}) & 0 & -\sin(\mathbf{q}\cdot\boldsymbol{\alpha}_{ni,mj})\\ 0 & 1 & 0\\ \sin(\mathbf{q}\cdot\boldsymbol{\alpha}_{ni,mj}) & 0 & \cos(\mathbf{q}\cdot\boldsymbol{\alpha}_{ni,mj})\end{pmatrix}\begin{pmatrix}S^x_{mj}\\ S^y_{mj}\\ S^z_{mj}\end{pmatrix}$$

$$\begin{aligned}=&-\sin(\mathbf{q}\cdot\boldsymbol{\alpha}_{ni,mj})[S^x_{ni}S^z_{mj}-S^z_{ni}S^x_{mj}]+\cos(\mathbf{q}\cdot\boldsymbol{\alpha}_{ni,mj})[S^x_{ni}S^x_{mj}-S^z_{ni}S^z_{mj}]\\&+S^y_{ni}S^y_{mj}.\end{aligned}\tag{8.2}$$

Hence, the Hamiltonian can be rewritten as

$$\begin{aligned}H'=\sum_{<ni,mj>}&(D_{ni,mj}-J_{ni,mj})\sin(\mathbf{q}\cdot\boldsymbol{\alpha}_{ni,mj})(S^x_{ni}S^z_{mj}-S^z_{ni}S^x_{mj})\\&+J_{ni,mj}\left[\cos(\mathbf{q}\cdot\boldsymbol{\alpha}_{ni,mj})(S^x_iS^x_j-S^z_iS^z_j).+S^y_{ni}S^y_{mj}\right]\end{aligned}\tag{8.3}$$

This is the rotated effective Hamiltonian, and the form of rotating around any axis can be derived similarly. Starting from the rotated Hamiltonian one can treat the system as that in the ferromagnetic state. This approach facilitates our later calculation.

8.2 Schwinger boson mean field theory

The application of the Schwinger boson (SB) method has been well studied in literature. We formulate our system by generalizing the method of Schwinger boson mean field theory (SBMFT). In the previous work such as Ref. [53] and Ref. [54], a technique applied on the antiferromagnetic system is to separate

doi:10.6342/NTU201901151

spins into two sublattices after introducing the Schwinger bosons. It has the adventage of highlighting order parameters. Mean-field approximation can be taken when a magnetic order is thought to be important and treated carefully. This point will be illustrated by our calculation below. We now have two types of boson operators a and b. Operator $a^\dagger(a)$ is a spin up creation (annihilation) operator, and $b^\dagger(b)$ is for spin down bosons. One can construct the spin states by such second quantization operators. The spin $1/2$ states, for example are, $|\uparrow\rangle = a^\dagger|0\rangle$, and $|\downarrow\rangle = b^\dagger|0\rangle$. Then there are following transformation for spin operators

$$\begin{aligned} S^+_{ni} &= a^\dagger_{ni} b_{ni}, \\ S^-_{ni} &= b^\dagger_{ni} a_{ni}, \\ S^z_{ni} &= \frac{1}{2}\left(a^\dagger_{ni} a_{ni} - b^\dagger_{ni} b_{ni}\right) \end{aligned} \tag{8.4}$$

for the $i-$th spin of the $n-$th unit cell. It is not hard to check such transformations satisfy all the commutation relations of bosons [55]. A constraint of the total spin number S on each site is imposed as

$$a^\dagger_{ni} a_{ni} + b^\dagger_{ni} b_{ni} = 2S, \tag{8.5}$$

where S is the total spin number. Thus, the Hamiltonian (8.2) in SB formulation after spin rotation is

$$\begin{aligned} H_{eff} = &\sum_{<ni,mj>} \left(\frac{J_{ni,mj} - J_{ni,mj}\cos\theta_{ni,mj} - D\epsilon_{ni,mj}\sin\theta_{ni,mj}}{4}\right) \widehat{A}^\dagger_{ni,mj}\widehat{A}_{ni,mj} \\ &+ \left(\frac{J_{ni,mj} + J_{ni,mj}\cos\theta_{ni,mj} + D\epsilon_{ni,mj}\sin\theta_{ni,mj}}{4}\right) \widehat{B}^\dagger_{ni,mj}\widehat{B}_{ni,mj} \\ &+ \left(\frac{D\epsilon_{ni,mj}\cos\theta_{ni,mj} - J_{ni,mj}\sin\theta_{ni,mj}}{4}\right) (\widehat{A}^\dagger_{ni,mj}\widehat{B}_{ni,mj} + \widehat{B}^\dagger_{ni,mj}\widehat{A}_{ni,mj}) \\ &+ \sum_{ni} \lambda_{ni}\left(a^\dagger_{ni} a_{ni} + b^\dagger_{ni} b_{ni} - 2S\right) \end{aligned} \tag{8.6}$$

where

$$\begin{aligned} \widehat{A}_{ni,mj} &= a_{ni} b^\dagger_{mj} - b_{ni} a^\dagger_{mj} \\ \widehat{B}_{ni,mj} &= a_{ni} a^\dagger_{mj} + b_{ni} b^\dagger_{mj} \end{aligned} \tag{8.7}$$

are the bond operators of two SB on two adjacent sites and $\theta_{ni,mj} = \mathbf{q}\cdot\boldsymbol{\alpha}_{ni,mj}$. Indices $< ni, mj >$ should be summed over all atoms in consideration. In this formulation, there are many atomic pairs. Physically, the system can be viewed as nearly ferromagnetic after spin rotation and we need only two

doi:10.6342/NTU201901151

kinds of mean fields in the system. As for field B, it describes the SB motion which always exists. Field A denotes an order parameter which deviates from ferromagnetic state. Its existence can be expected as the spins in our system are frustrated due to various couplings. The mean field value $A(B) = \langle \widehat{A}(\widehat{B})_{ni,mj} \rangle$ is evaluated with the states after rotation, which are the two of three the main parameters we are going to solve The way to take mean field approximation of operator $\widehat{B}$ is

$$\begin{aligned} \widehat{B}^{\dagger}_{ni,mj}\widehat{B}_{ni,mj} &\cong (\widehat{B}^{\dagger}_{ni,mj} + \widehat{B}_{ni,mj})\langle \widehat{B}_{ni,mj} \rangle - \langle \widehat{B}_{ni,mj} \rangle^2 \\ &= (\widehat{B}^{\dagger}_{ni,mj} + \widehat{B}_{ni,mj})B - B^2, \end{aligned} \tag{8.8}$$

where all $\langle \widehat{B}_{ni,mj} \rangle = B$. The mean field of operator $\widehat{A}_{ni,mj}$ should be treat more carefully. One can see that as ni and mj exchange positions, $\widehat{A}_{mj,ni} = -\widehat{A}^{\dagger}_{ni,mj}$. In general, mean field $\langle \widehat{A}_{ni,mj} \rangle$ behaves like $iAe^{i\phi\epsilon_{ni,mj}}$. The value of phase ϕ can be determined to get lowest ground state energy. The final approximation is letting all $\lambda_{ni} = \lambda$ which represents a Lagrange multiplier. We then take Fourier transform of operator $\widehat{A}(\widehat{B})_{ni,mj}$. The spin up Schwinger boson operator a is transfered as

$$a_{ni} = \frac{1}{\sqrt{N}} \sum_{\mathbf{k}}^{B.Z} a_{i,\mathbf{k}} e^{-i\mathbf{k}\cdot\mathbf{R}_n} = \frac{1}{\sqrt{N}} \sum_{\mathbf{k}}^{B.Z} a_{\mathbf{k}} e^{-i\mathbf{k}\cdot\mathbf{R}_n}.$$

A similar transform is also valid for operator b_{ni}. $\mathbf{R}_n$ indicates the origin of nth cell as mentioned before, and N is the number of spins for sublattice i and also, the total number of unit cell. Furthermore, the $a_{ni,\mathbf{k}}$ is independent of i since the spins are parallel after rotation. We, therefore, dropped the subscript i. The mean-field Hamiltonian in momentum space is

$$\begin{aligned} H_{MF} = \sum_{\mathbf{k}}^{B.Z} \Big[&(-i\gamma_1(\mathbf{k})A + i\gamma_{ss}(\mathbf{k})B)(a^{\dagger}_{\mathbf{k}} b_{\mathbf{k}} - b^{\dagger}_{\mathbf{k}} a_{\mathbf{k}}) + \\ &(\lambda + \gamma_2(\mathbf{k})B - \gamma_{sc}(\mathbf{k})A)(a^{\dagger}_{\mathbf{k}} a_{\mathbf{k}} + b^{\dagger}_{\mathbf{k}} b_{\mathbf{k}}) \Big] + E_0(A, B, \lambda), \end{aligned} \tag{8.9}$$

doi:10.6342/NTU201901151

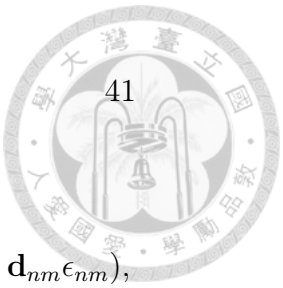

where

$$\begin{aligned}
\gamma_1(\mathbf{k}) &= \sum_{<ni,mj>} \frac{1}{2}\left[J_{ni,mj}(1-\cos\theta_{ni,mj}) - D\epsilon_{ni,mj}\sin\theta_{ni,mj}\right]\sin(\mathbf{k}\cdot\mathbf{d}_{nm}\epsilon_{nm}),\\
\gamma_{ss}(\mathbf{k}) &= \sum_{<ni,mj>} \frac{1}{2}\left[J_{ni,mj}\sin\theta_{ni,mj} - D\epsilon_{ni,mj}\cos\theta_{ni,mj}\right]\sin(\mathbf{k}\cdot\mathbf{d}_{nm}),\\
\gamma_2(\mathbf{k}) &= \sum_{<ni,mj>} \frac{1}{2}\left[J_{ni,mj}(1+\cos\theta_{ni,mj}) + D\epsilon_{ni,mj}\sin\theta_{ni,mj}\right]\sin(\mathbf{k}\cdot\mathbf{d}_{nm}\epsilon_{nm}),\\
\gamma_{sc}(\mathbf{k}) &= \sum_{<ni,mj>} \frac{1}{2}\left[J_{ni,mj}\sin|\theta_{ni,mj}| - D\epsilon_{ni,mj}\cos\theta_{ni,mj}\right]\cos(\mathbf{k}\cdot\mathbf{d}_{nm}\epsilon_{nm}),
\end{aligned} \tag{8.10}$$

and

$$\begin{aligned}
\frac{E_0}{N} &= -\frac{1}{4}\sum_{<ni,mj>}\left[J_{ni,mj}(1-\cos\theta_{ni,mj}) - D\epsilon_{ni,mj}\sin\theta_{ni,mj}\right]A^2 +\\
&\left[J_{ni,mj}(1+\cos\theta_{ni,mj}) + D\epsilon_{ni,mj}\sin\theta_{ni,mj}\right]B^2 + (D\cos\theta_{ni,mj} +\\
&J_{ni,mj}\epsilon_{ni,mj}\sin\theta_{ni,mj})\,2AB - \lambda(2S)\\
&\equiv -J_- A^2 - J_+ B^2 + 2J_s AB - \lambda(2S).
\end{aligned} \tag{8.11}$$

Summation of $\mathbf{k}$ is over the first Brillouin zone. Vector $\mathbf{d}_{nm}$ in (8.10) denotes the difference between the nth and mth unit cells. For example, $\mathbf{d}_{n1,n2} = \mathbf{0}$ and $\mathbf{d}_{n1,m2} = \mathbf{R}_m - \mathbf{R}_n$. $\boldsymbol{\alpha}_{ni,mj}$ may or may not be equal to $\mathbf{d}_{nm}$, depending on the type of crystal structure.

We diagonalize the Hamiltonian of Eq.(8.9) by the Bogoliubov transformation

$$\begin{aligned}
a_{\mathbf{k}} &= \cos\theta_{\mathbf{k}}\alpha_{\mathbf{k}} + i\sin\theta_{\mathbf{k}}\beta_{\mathbf{k}}\\
b_{\mathbf{k}} &= \cos\theta_{\mathbf{k}}\beta_{\mathbf{k}} + i\sin\theta_{\mathbf{k}}\alpha_{\mathbf{k}}.
\end{aligned} \tag{8.12}$$

It is not hard to show that the condition $\cos^2\theta_{\mathbf{k}} = \sin^2\theta_{\mathbf{k}}$ should be satisfied. We choose $\theta_{\mathbf{k}} = \frac{\pi}{4}$ without losing generality. The mean field Hamiltonian becomes

$$H_{MF} = \sum_{\mathbf{k}}^{B.Z}(\lambda + \omega_{2\mathbf{k}} - \omega_{1\mathbf{k}})\alpha_{\mathbf{k}}^\dagger\alpha_{\mathbf{k}} + (\lambda + \omega_{2\mathbf{k}} + \omega_{1\mathbf{k}})\beta_{\mathbf{k}}^\dagger\beta_{\mathbf{k}} + E_0, \tag{8.13}$$

where $\omega_{1\mathbf{k}} = -\gamma_1(\mathbf{k})A + \gamma_{ss}(\mathbf{k})B$ and $\omega_{2\mathbf{k}} = \gamma_2(\mathbf{k})B - \gamma_{sc}(\mathbf{k})A$.

doi:10.6342/NTU201901151

8.3 Free Energy and SB Equations

The analysis of thermodynamic property is standard. With Hamiltonian (8.13), we have the mean-field partition function $Q_{MF} = Tr[\exp(-\beta H_{MF})]$ and the free energy is

$$F = -\frac{1}{\beta}\ln Q_{MF} = -\frac{1}{\beta}\sum_{\mathbf{k}}[\ln(1+n_{\alpha\mathbf{k}}) + \ln(1+n_{\beta\mathbf{k}})] + E_0, \tag{8.14}$$

where $n_{\mathbf{k}\alpha(\beta)} = (\exp[\beta(\lambda + \omega_{2\mathbf{k}} - (+)\omega_{1\mathbf{k}})] - 1)^{-1}$ is the Bose-Einstein distribution of the Schwinger boson quasi-particles.

A set of self-consistent equations are acquired by minimizing the free energy (8.14) respective to parameters A, B, and λ. Hence, the self-consistent SB equations can be simplified as

$$\begin{aligned} 2S &= \frac{1}{N}\sum_{\mathbf{k}} n_{\mathbf{k},\alpha} + n_{\mathbf{k},\beta} \\ -2J_- A + 2J_s B &= \frac{1}{N}\sum_{\mathbf{k}} (n_{\mathbf{k},\alpha} - n_{\mathbf{k},\beta})\gamma_1(\mathbf{k}) - (n_{\mathbf{k},\alpha} + n_{\mathbf{k},\beta})\gamma_{sc}(\mathbf{k}) \\ -2J_+ A + 2J_s B &= \frac{1}{N}\sum_{\mathbf{k}} (n_{\mathbf{k},\alpha} + n_{\mathbf{k},\beta})\gamma_2(\mathbf{k}) + (n_{\mathbf{k},\beta} + n_{\mathbf{k},\alpha})\gamma_{ss}(\mathbf{k}). \end{aligned} \tag{8.15}$$

The forms of J_-, J_+, and J_s are defined in Eq.(8.11). In view of the first equation of Eqs.(8.15), one must have macroscopic number of SB occupying a lowest energy state. The lowest energy states, denoted by $\mathbf{k} = \pm\mathbf{k}_0$ are determined by the value of λ. Here, we suggest the possibility of condensation at finite $\mathbf{k}_0$. In previous works such as Ref. [54], it was suggested that condensation occurs at $\mathbf{k} = 0$.

We choose λ as the value to make the minima of $\lambda + \omega_{2,\mathbf{k}} \pm \omega_{1,\mathbf{k}}$ equal to zero. Then we set $\mathbf{k} = \mathbf{k}_0$ for minimum $\lambda + \omega_{2,\mathbf{k}} + \omega_{1,\mathbf{k}}$. One can observe that ω_1 is odd whilst ω_2 is even in $\mathbf{k}$. It means that the energy $\omega_2(\mathbf{k}) + \omega_1(\mathbf{k}) = \omega_2(\mathbf{k}) - \omega_1(-\mathbf{k})$ in $\mathbf{k} \in B.Z.$ The minimum of $\lambda + \omega_2 + \omega_1$ and $\lambda + \omega_2 - \omega_1$ are symmetric with respect to $\mathbf{k} = 0$. In other words, if one find that the minimum of $\lambda + \omega_2 + \omega_1$ is at some $\mathbf{k}_0$, the minimum of $\lambda + \omega_2 - \omega_1$ is at $-\mathbf{k}_0$. Thus, for $T < T_c$, the equations can be rewritten in terms of $n_{\mathbf{k},\beta}$.

doi:10.6342/NTU201901151

$$
\begin{aligned}
S &= \frac{1}{N}\sum_{\mathbf{k}\neq\mathbf{k}_0} n_{\mathbf{k},\beta} + n_0 \\
-J_- A + J_s B &= -\frac{1}{N}\sum_{\mathbf{k}\neq\mathbf{k}_0} n_{\mathbf{k},\beta}(\gamma_1(\mathbf{k}) + \gamma_{sc}(\mathbf{k})) - n_0(\gamma_1(\mathbf{k}_0) + \gamma_{sc}(\mathbf{k}_0)) \\
-J_+ A + J_s B &= \frac{1}{N}\sum_{\mathbf{k}\neq\mathbf{k}_0} n_{\mathbf{k},\beta}(\gamma_2(\mathbf{k}_0) - \gamma_{ss}(\mathbf{k}_0)) + n_0(\gamma_2(\mathbf{k}_0) - \gamma_{ss}(\mathbf{k}_0)).
\end{aligned}
\tag{8.16}
$$

The unknown parameters to be solved are A and B. Constant n_0, the condensation density, is necessary since a macroscopic number of Schwinger bosons are condensed at $\mathbf{k} = \pm\mathbf{k}_0$ as $T < T_c$. n_0 represents the density at $\mathbf{k} = \mathbf{k}_0$ and its physical meaning is the magnetic moment of the system. The summation is for all $\mathbf{k}$ except $\mathbf{k}_0$. One can say the long-range order (LRO) is interpreted as the Bose Einstein condensation of SB. Therefore, we have to solve A, B and identify n_0 when $T < T_c$. One should keep in mind that the set of equations (8.16) are valid only if $\mathbf{q} = \mathbf{Q}_c$, the commensurate magnetic configuration vector. Incommensurate spin configuration, however, violates the periodic boundary condition and the spins need infinite number of lattice sites to "rotate back". The way to deal with incommensurate spin is to expand $\mathbf{Q}_{ic}$ near $\mathbf{Q}_c$. We will discuss it further in Ch. 10.

doi:10.6342/NTU201901151

doi:10.6342/NTU201901151

Chapter 9

Application of SBMFT to CuO

9.1 The information of CuO

Now let's turn our attention to the structure of CuO. Following the choice of magnetic unit cell in [52], our basis of an unit cell are $\mathbf{t}_1 = (a, 0, c), \mathbf{t}_2 = (0, -b, 0), \mathbf{t}_3 = (a, 0, -c)$, instead of the common *abc*-coordinate, see FIG. 9.1 The location of Cu atoms in a unit cell in $\mathbf{t}_i$ representation are $\mathbf{r}_1 = (\frac{1}{8}, -\frac{1}{4}, \frac{1}{8})$, $\mathbf{r}_2 = (\frac{3}{8}, -\frac{3}{4}, \frac{3}{8})$, $\mathbf{r}_3 = (\frac{3}{8}, -\frac{3}{4}, \frac{-1}{8})$, $\mathbf{r}_4 = (\frac{-1}{8}, -\frac{3}{4}, \frac{3}{8})$, $\mathbf{r}_5 = (\frac{-1}{8}, -\frac{3}{4}, \frac{-1}{8})$, $\mathbf{r}_6 = (\frac{-3}{8}, -\frac{1}{4}, \frac{-3}{8})$, $\mathbf{r}_7 = (\frac{1}{8}, -\frac{1}{4}, \frac{-3}{8})$, $\mathbf{r}_8 = (\frac{-3}{8}, -\frac{1}{4}, \frac{1}{8})$. For example, $\mathbf{r}_1 = \frac{1}{8}\mathbf{t}_1 - \frac{1}{4}\mathbf{t}_2 + \frac{1}{8}\mathbf{t}_3$, and $\mathbf{r}_2 = \frac{3}{8}\mathbf{t}_1 - \frac{1}{4}\mathbf{t}_2 + \frac{1}{8}\mathbf{t}_3$. The primitive lattice vectors in reciprocal space are $\mathbf{g}_1 = (\frac{\pi}{a}, 0, \frac{\pi}{c})$, $\mathbf{g}_2 = (0, -\frac{2\pi}{b}, 0)$, $\mathbf{g}_3 = (\frac{\pi}{a}, 0, \frac{-\pi}{c})$, and $\mathbf{k}$ is written as $k_1\mathbf{g}_1 + k_2\mathbf{g}_2 + k_3\mathbf{g}_3$. The corresponding interaction between two spins are listed in Table 9.1 The energy magnitude is measured relative to the largest interaction J_3 throughout the entire article. Their relative strength are $(J_3, J_1, J_a, J_b, J_2) = (1, -0.325, -0.1, 0.3, 0.35)$ [48] and the strength of DM interaction $D = 0.0125J_3$.

The relative vectors of nearest neighboring unit cells $\mathbf{d}_{nm}$ are shown in the following matrix form. They will be used in Eq.(8.10)

$\mathbf{d}_{nm} =$

$$\begin{bmatrix}
0 & \mathbf{t}_3 & 0 & \mathbf{t}_1 & 0 & \mathbf{t}_2 & 0 & \mathbf{t}_2 & 0 & \mathbf{t}_2 & 0 & \mathbf{t}_1+\mathbf{t}_3 \\
0 & \mathbf{t}_3 & 0 & \mathbf{t}_1 & \mathbf{t}_1 & \mathbf{t}_1-\mathbf{t}_2 & \mathbf{t}_3 & -\mathbf{t}_2+\mathbf{t}_3 & 0 & \mathbf{t}_1-\mathbf{t}_2+\mathbf{t}_3 & 0 & \mathbf{t}_1+\mathbf{t}_3 \\
0 & -\mathbf{t}_3 & 0 & \mathbf{t}_1 & \mathbf{t}_1 & \mathbf{t}_1-\mathbf{t}_2 & 0 & -\mathbf{t}_2 & -\mathbf{t}_2 & \mathbf{t}_1 & -\mathbf{t}_3 & \mathbf{t}_1 \\
0 & \mathbf{t}_3 & 0 & -\mathbf{t}_1 & 0 & -\mathbf{t}_2 & \mathbf{t}_3 & -\mathbf{t}_2+\mathbf{t}_3 & -\mathbf{t}_2 & \mathbf{t}_3 & -\mathbf{t}_1 & \mathbf{t}_3 \\
0 & -\mathbf{t}_3 & 0 & -\mathbf{t}_1 & 0 & -\mathbf{t}_2 & 0 & -\mathbf{t}_2 & 0 & -\mathbf{t}_2 & -\mathbf{t}_1-\mathbf{t}_3 & 0 \\
0 & -\mathbf{t}_3 & 0 & -\mathbf{t}_1 & -\mathbf{t}_1 & -\mathbf{t}_1+\mathbf{t}_2 & -\mathbf{t}_3 & \mathbf{t}_2-\mathbf{t}_3 & 0 & -\mathbf{t}_1+\mathbf{t}_2-\mathbf{t}_3 & -\mathbf{t}_1-\mathbf{t}_3 & 0 \\
0 & -\mathbf{t}_3 & 0 & \mathbf{t}_1 & 0 & \mathbf{t}_2 & -\mathbf{t}_3 & \mathbf{t}_2-\mathbf{t}_3 & \mathbf{t}_2 & -\mathbf{t}_3 & -\mathbf{t}_3 & \mathbf{t}_1 \\
0 & \mathbf{t}_3 & 0 & -\mathbf{t}_1 & -\mathbf{t}_1 & -\mathbf{t}_1+\mathbf{t}_2 & 0 & \mathbf{t}_2 & \mathbf{t}_2 & -\mathbf{t}_1 & -\mathbf{t}_1 & \mathbf{t}_3
\end{bmatrix}$$

There are two wave vectors representing the commensurate and incommensurate phase of CuO, $\mathbf{Q}_c = \mathbf{g}_3$ and $\mathbf{Q}_{ic} = 0.023\mathbf{g}_1 + 0.989\mathbf{g}_3$, respectively. (In *abc*-coordinate, $\mathbf{Q}_c = (0.5, 0, -0.5)$ and $\mathbf{Q}_{ic} = (0.506, 0, -0.483)$ [44]). Below

doi:10.6342/NTU201901151

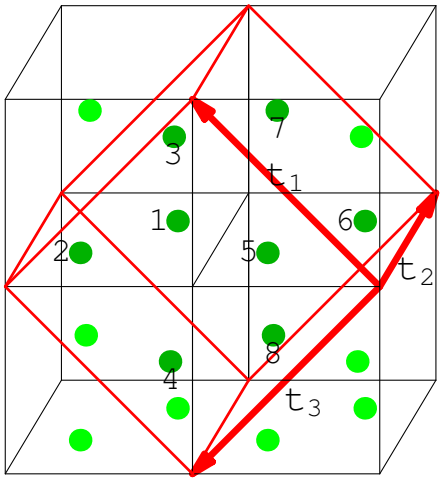

Figure 9.1: Illustration of the magnetic unit cell and the positions of copper atoms

T_{N1}, the system is in colinear phase with commensurate magnetic configuration vector $\mathbf{Q}_c$, whilst incommensurate $\mathbf{Q}_{ic}$ corresponds to spiral spin phase in the temperature range 213K$\sim$230K.

First we briefly explain the work of Ref.[52]. They considered the irreducible representations of τ_1 and τ_2 of paramagnetic space group $C2/c1'$ in the commensurate phase. There are two two-component order parameters $(\eta_1 = \rho_1 \cos\theta_1, \eta_2 = \rho_1 \sin\theta_1)$ and $(\zeta_1 = \rho_2 \cos\theta_2, \zeta_2 = \rho_2 \sin\theta_2)$ associated with $\mathbf{Q}_c = \pm(0, 5, 0, -0.5)$. These parameters are coupled by the relation of Landau free energy, see Eq.(1) of Ref.[52]. Minimizing the Landau free energy they have 11 possible stable phases for different equilibrium value of ρ_1, ρ_2, θ_1 and θ_2, see TABLE. II of Ref.[52]. Considering the experimental results phase IV is chosen. This phase leads to a condition of equilibrium $\eta_1^{a,b,c} = \eta_2^{a,b,c} = 0$, $\zeta_1^{a,b,c} = -\zeta_2^{a,b,c}$ and antitranslational relationships $\vec{s_1} = -\vec{s_6}$, $\vec{s_2} = -\vec{s_5}$, $\vec{s_3} = -\vec{s_4}$, $\vec{s_7} = -\vec{s_8}$. So the commensurate spin configurations of Ref.[52] are

$$s_1^{ac} = s_4^{ac} = s_5^{ac} = s_7^{ac} = -s_2^{ac} = -s_3^{ac} = -s_6^{ac} = -s_8^{ac}$$
$$s_1^{b} = s_3^{b} = s_5^{b} = s_8^{b} = -s_2^{b} = -s_4^{b} = -s_6^{b} = -s_7^{b}.$$

We then demonstrate our choice of spin configuration for commensurate phase. According to the magnetic modulation vector $\mathbf{Q}_c$, we can identify the relative angles between two spins. In the paper of neutron scattering study, the component of spins along $\mathbf{g}_2$ (or b-axis) direction is more certain [52]. Our strategy is, assuming the spin component along b-axis is determined, those

doi:10.6342/NTU201901151

Table 9.1:

Cu	1	2	3	4	5	6	7	8
J_3	7	3	2	5	4	8	1	6
J_3	$7_{\mathbf{t}_3}$	$3_{\mathbf{t}_3}$	$2_{-\mathbf{t}_3}$	$5_{\mathbf{t}_3}$	$4_{-\mathbf{t}_3}$	$8_{-\mathbf{t}_3}$	$1_{-\mathbf{t}_3}$	$6_{\mathbf{t}_3}$
J_1	8	4	5	2	3	7	6	1
J_1	$8_{\mathbf{t}_1}$	$4_{\mathbf{t}_1}$	$5_{\mathbf{t}_1}$	$2_{-\mathbf{t}_1}$	$3_{-\mathbf{t}_1}$	$7_{-\mathbf{t}_1}$	$6_{\mathbf{t}_1}$	$1_{-\mathbf{t}_1}$
J_b	4	$8_{\mathbf{t}_1}$	$6_{\mathbf{t}_1}$	1	7	$3_{-\mathbf{t}_1}$	5	$2_{-\mathbf{t}_1}$
J_b	$4_{\mathbf{t}_2}$	$8_{\mathbf{t}_1-\mathbf{t}_2}$	$6_{\mathbf{t}_1-\mathbf{t}_2}$	$1_{-\mathbf{t}_2}$	$7_{-\mathbf{t}_2}$	$3_{-\mathbf{t}_1+\mathbf{t}_2}$	$5_{\mathbf{t}_2}$	$2_{-\mathbf{t}_1+\mathbf{t}_2}$
J_b	3	$7_{\mathbf{t}_3}$	1	$6_{\mathbf{t}_3}$	8	$4_{-\mathbf{t}_3}$	$2_{-\mathbf{t}_3}$	5
J_b	$3_{\mathbf{t}_2}$	$7_{-\mathbf{t}_2+\mathbf{t}_3}$	$1_{-\mathbf{t}_2}$	$6_{-\mathbf{t}_2+\mathbf{t}_3}$	$8_{-\mathbf{t}_2}$	$4_{\mathbf{t}_2-\mathbf{t}_3}$	$2_{\mathbf{t}_2-\mathbf{t}_3}$	$5_{\mathbf{t}_2}$
J_a	2	1	$7_{-\mathbf{t}_2}$	$8_{-\mathbf{t}_2}$	6	5	$3_{\mathbf{t}_2}$	$4_{\mathbf{t}_2}$
J_a	$5_{\mathbf{t}_2}$	$6_{\mathbf{t}_1-\mathbf{t}_2+\mathbf{t}_3}$	$8_{\mathbf{t}_1}$	$7_{\mathbf{t}_3}$	$1_{-\mathbf{t}_2}$	$2_{-\mathbf{t}_1+\mathbf{t}_2-\mathbf{t}_3}$	$4_{-\mathbf{t}_3}$	$3_{-\mathbf{t}_1}$
J_2	6	5	$4_{-\mathbf{t}_3}$	$3_{-\mathbf{t}_1}$	$2_{-\mathbf{t}_1-\mathbf{t}_3}$	$1_{-\mathbf{t}_1-\mathbf{t}_3}$	$8_{-\mathbf{t}_3}$	$7_{-\mathbf{t}_2}$
J_2	$6_{\mathbf{t}_1+\mathbf{t}_3}$	$5_{\mathbf{t}_1+\mathbf{t}_3}$	$4_{\mathbf{t}_1}$	$3_{\mathbf{t}_3}$	2	1	$8_{\mathbf{t}_1}$	$7_{\mathbf{t}_3}$

This table gives the coupling constants between two copper atoms. Numbers $1\sim 8$ denote the Cu atoms in n-th unit cell. The vector in subscript of each number indicates the position vector of the unit cell where Cu atoms are located, ex: $7_{\mathbf{t}_1}$ means the position of the $7th$ atom is $\mathbf{r}_7+\mathbf{t}_1$. Those without subscript are the atoms in the unit cell containing the origin.

in the a and c directions can be obtained by the relative angles between two spins. For instance, angle between the spins of Cu1 and Cu7 is π, and for Cu1 and Cu2 is $\pi/2$. For instance, $s_1^b=-s_2^b$ leads to $s_1^{ac}=s_2^{ac}$ since the angle is $\pi/2$, see FIG. 9.2. Hence, our spin configuration for commensurate phase is

$$\begin{aligned} &s_1^{ac}=s_2^{ac}=s_4^{ac}=s_8^{ac}=-s_3^{ac}=-s_5^{ac}=-s_6^{ac}=-s_7^{ac} \\ &s_1^{b}=s_3^{b}=s_5^{b}=s_8^{b}=-s_2^{b}=-s_4^{b}=-s_6^{b}=-s_7^{b} \end{aligned} \tag{9.1}$$

The advantages of this spin configuration are: First, it is consistent with the experimental [47] results; Second, the configuration has the lowest ground state energy, at least classically. For example, the spins on 1-7-1 chains is now completely anti-parallel, and they have the strongest AFM interaction J_3 [47]. Third, it also satisfies the symmetry properties of group theory suggest by [52] which we mentioned before. Thus we believe the actual spin configuration is more likely to be the one in Eq.(9.1). We thus proceed to diagonalized the Hamiltonian in Eq. (8.2) based on the spin configuration Eq.(9.1). The rotation is such that all the spins $s_1\sim s_8$ are pointed to the z-direction in local coordinates. $\theta_{ni,mj}$ in Eq.(8.6) now is equal to $\mathbf{Q}_c\cdot\boldsymbol{\alpha}_{ni,mj}$

doi:10.6342/NTU201901151

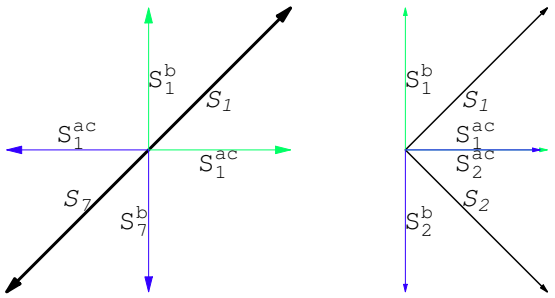

Figure 9.2: The determination spin directions. Take spin 1 and 7 as an example, we know their angle is π by $\mathbf{Q}_c$. We also know that $s_1^b = -s_7^b$ by neutron scattering. Thus, we know $s_1^{ac} = -s_7^{ac}$ as shown in *l.h.s* of FIG. 9.2. A similar method is applied to the other spins. For example, spin 1 and 2 has $\mathbf{Q}_c \cdot \boldsymbol{\alpha}_{12} = \pi/2$. Thus we conclude $s_1^b = -s_2^b$ and $s_1^{ac} = s_2^{ac}$.

9.2 Finite momentum BEC of magnon

In this section, we compare the magnon condensation of CuO between former works of finite momentum BEC in magnetic systems. Theoretical argument of interacting boson showing possible finite momentum condensate is suggest by [5], as we mentioned in the exordium. However, the realization of such BEC is observed in only past two decades.

Finite momentum condensation were observed by experiments. The first experimental report is the magnetic insulator $TlCuCl_3$ [56]. How can one tell that the condensate of $TlCuCl_3$ has finite momentum? The system has state of singlet spins with Cu^{2+} ions forming dimers. The excited state is a triplet with spin 1. There is an energy gap for magnons. The $S_z = 1$ state is coupled with external magnetic field and hence, we can use an external field to tune the magnitude of the energy gap. Eventually the system shows long range order (LRO) and we can measure the temperature-dependent field strength. They interpret this is the condensation of $S_z = 1$ magnons.

Another important experiment of magnons is in YIG films [57]. Magnons are pumped into the system using microwaves. The measurement of final state is achieved via laser light which is inelastically scattered by magnons. This experiment relies on the difference in relaxation times between non-equilibrium magnons and the thermalized magnon. Instead of measuring the energy change, another way is to measure the behavior of momentum.

CuO also demonstrate similar momentum behavior. In FIG. 9.3, we plot the energy dispersion relation $\omega_{\beta,\mathbf{k}} \equiv \lambda + \omega_{1\mathbf{k}} + \omega_{2\mathbf{k}}$ of CuO. Let $k_3 = 0.118$,

doi:10.6342/NTU201901151

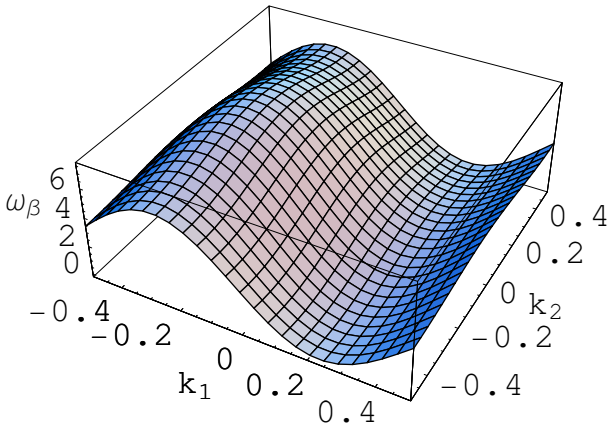

Figure 9.3: The dispersion relation of $\omega_{\beta,\mathbf{k}}$ at $T = J_3/4$ and $k_3 = 0.118$. The magnitude of energy is relative to J_3.

the 3rd component of minimum $\mathbf{k}_0$ at temperature $T = J_3/4$. It shows that the minimum of $\omega_{\beta,\mathbf{k}}$ at $\mathbf{k}_0 = 0.229\mathbf{g}_1 - 0.347\mathbf{g}_2 + 0.118\mathbf{g}_3$. This is where BEC situated. The other minimum of $\omega_{\alpha,\mathbf{k}} \equiv \lambda + \omega_{1\mathbf{k}} - \omega_{2\mathbf{k}}$ is at $-\mathbf{k}_0$. As for $\mathbf{k} = 0$, the energy $\omega_{\alpha,0} = \omega_{\beta,0}$. In a material such as CuO, we suggest that there will be a peak if we measure the cross section of neutron scattering. The change of momentum of incident and reflected beams should be at $\pm\mathbf{Q}_c \pm \mathbf{k}_0$. This is an evidence of the finite momentum BEC of quasi-particles. Physically the magnetic ordering linked with magnon condensation which is analogous to conventional BEC (BEC of bosons) despite the lowest energy state is composited by finite momentum wave-functions.

9.3 The spin correlation function

In order to compare our theoretical model for CuO with experimental results, we calculate the spin correlation function with spins directions both vertical and parallel to our SB rotation axis. The correlations contain many physically measurable quantities. In a magnetic spin system, one of important experimental results is magnetic susceptibility. In our SB model, the rotation axis of Hamiltonian is y-axis, which corresponds to the linear combination of a and c coordinates of [52]. Hence χ^a and χ^c contain part of $\sum\langle S^y S^y\rangle$. It is not hard to understand the spin correlation function of y axis is invariant before and after rotation of the Hamiltonian.

doi:10.6342/NTU201901151

$$\sum_{n,m}\langle S'^{y}_{n}S'^{y}_{m}\rangle = \sum_{n,m}\langle S^{y}_{n}S^{y}_{m}\rangle$$
$$= -\frac{1}{4}\sum_{n,m,\mathbf{k}_1\sim\mathbf{k}_4}\langle(a^{\dagger}_{\mathbf{k}_1}b_{\mathbf{k}_2}-b^{\dagger}_{\mathbf{k}_1}a_{\mathbf{k}_2})(a^{\dagger}_{\mathbf{k}_3}b_{\mathbf{k}_4}-b^{\dagger}_{\mathbf{k}_3}a_{\mathbf{k}_4})e^{i\mathbf{R}_n\cdot(\mathbf{k}_2-\mathbf{k}_1)}e^{i\mathbf{R}_m\cdot(\mathbf{k}_4-\mathbf{k}_3)}\rangle. \tag{9.2}$$

With the Bogoliubov transformation in Eq.(8.12), we consider the momentum $\mathbf{k}=\pm\mathbf{k}_0$ independently, where particles $\alpha_{\mathbf{k}}$ condensed at $-\mathbf{k}_0$ and particles $\beta_{\mathbf{k}}$ condensed at $\mathbf{k}_0$. The full expansion of Eq. (9.2) is

$$\begin{aligned}\frac{1}{16N^2}\sum_{n,m,\mathbf{k}_1\sim\mathbf{k}_4}&\langle\alpha^{\dagger}_1\alpha_2\alpha^{\dagger}_3\alpha_4-\alpha^{\dagger}_1\alpha_2\beta^{\dagger}_3\beta_4-\alpha^{\dagger}_1\alpha_2\beta^{\dagger}_4\beta_3+\beta^{\dagger}_3\beta_4\alpha^{\dagger}_4\alpha_3\\ &-\beta^{\dagger}_1\beta_2\alpha^{\dagger}_3\alpha_4+\beta^{\dagger}_1\beta_2\beta^{\dagger}_3\beta_4+\beta^{\dagger}_1\beta_2\beta^{\dagger}_4\beta_3-\beta^{\dagger}_1\beta_2\alpha^{\dagger}_4\alpha_3\\ &-\beta^{\dagger}_2\beta_1\alpha^{\dagger}_3\alpha_4+\beta^{\dagger}_2\beta_1\beta^{\dagger}_3\beta_4+\beta^{\dagger}_2\beta_1\beta^{\dagger}_4\beta_3-\beta^{\dagger}_2\beta_1\alpha^{\dagger}_4\alpha_3\\ &+\alpha^{\dagger}_2\alpha_1\alpha^{\dagger}_3\alpha_4-\alpha^{\dagger}_2\alpha_1\beta^{\dagger}_3\beta_4-\alpha^{\dagger}_2\alpha_1\beta^{\dagger}_4\beta_3+\alpha^{\dagger}_2\alpha_1\alpha^{\dagger}_4\alpha_3\rangle\\ &\cdot e^{i\mathbf{R}_n\cdot(\mathbf{k}_2-\mathbf{k}_1)}e^{i\mathbf{R}_m\cdot(\mathbf{k}_4-\mathbf{k}_3)}.\end{aligned} \tag{9.3}$$

For $\mathbf{k}_1=\mathbf{k}_2=\mathbf{k}_3=\mathbf{k}_4=-\mathbf{k}_0$, the particles $\alpha_{\mathbf{k}}$ condensed but particles $\beta_{\mathbf{k}}$ do not. This yields $4\langle\alpha^{\dagger}_0\alpha_0\alpha^{\dagger}_0\alpha_0\rangle = 4n^2_{0,\alpha}$. On the other hand, we have $4\langle\beta^{\dagger}_0\beta_0\beta^{\dagger}_0\beta_0\rangle = 4n^2_{0,\beta}$ as all $\mathbf{k}'s$ equals to $\mathbf{k}_0$. We can further simplify the notation as $n^2_{0,\alpha}=n^2_{0,\beta}=n^2_0$ according to Eq. (16a). Thus, we obtain the magnetic susceptibility function χ^y as

$$\chi^y = \frac{g\mu_B}{2V}\left[\frac{n^2_0}{2}+\frac{1}{2N}\sum_{\mathbf{k}\neq\mathbf{k}_0}n_{\mathbf{k}}(n_{\mathbf{k}}+1)-\frac{1}{N}\sum_{\mathbf{k},\mathbf{k}'\neq\mathbf{k}_0}n_{\mathbf{k}}n_{\mathbf{k}'}\right]. \tag{9.4}$$

It approaches a finite value $\frac{g\mu_B}{4V}n^2_0$ as $T\to 0$. As both χ^a and χ^c contain part of χ^y, they also approach a finite constant as $T\to 0$. This agrees with experimental result [47]. Physically, consider the spiral spins lie on a plane formed by vectors $\vec{b}$ and $\vec{a}+\vec{c}$. Any perpendicular external field, even slightly, will lead a significant change of magnetic moment. Our $y-$axis is a linear combination a and c so that χ^y corresponds to a average of χ^a and χ^c. This fact is shown in the experimental measurement [47]. Our model can, at least qualitatively, describes this result.

As for susceptibility χ^b, for which the dc magnetic field is applied along $b-$axis or perpendicular to the spiral axis. The BEC density does not have contribution. As a result χ^b approaches zero when $T\to 0$. We found that, some anisotropic energy on the spiral plane has to be added to our calculation

doi:10.6342/NTU201901151

in order to compare the experimental data. This will add unnecessary complication to our computation. Hence we did not go further in this direction so as to present a clear physical picture.

doi:10.6342/NTU201901151

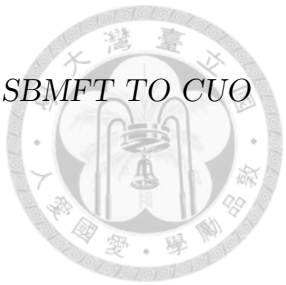

doi:10.6342/NTU201901151

Chapter 10

The c-ic Phase Transition of CuO

In this chapter, we explain how the transition occurs between commensurate and incommensurate $c-ic$ phases. A straightforward and convincing way is to compare the free energy $F = U - TS$ of two phases. One can imagine the system prefers commensurate phase when free energy F_c is smaller than the incommensurate free energy F_{ic} at low temperature. As temperature increases, F_{ic} becomes smaller and the system move into incommensurate phase. Mathematically, we are going to look for a temperature T_{c-ic} which satisfies the equation

$$F_{ic} - F_c = U_{ic} - U_c - T_{c-ic}\Delta S = 0. \tag{10.1}$$

In this circumstance, the free energy obtained from SBMFT before is not enough since a more sophisticated incommensurate phase should be considered. What comes in is not the absolute entropy but the difference of entropies between commensurate and incommensurate phase. Now we interpret the free energy in (8.14) as the internal energy U. Solving parameters A, B and λ in Eq.(8.16) for a given temperature, then feed these values into Eq.(8.14) to get U_c. For U_{ic}, as mentioned before, we expand the energy functions with respect to Q_c up to the second order of $Q_{ic} - Q_c$ and we insert the (A, B, λ) which is obtained from commensurate equations (8.16). We have the value of $U_{ic} - U_c$ which tends to be $0.0185J_3$ at low temperature. Thus, the spins prefer commensurate configuration at low T.

The main feature of entropy and the magnetic modulation vector Q can be understood in terms of a soliton model. We illustrate our calculation by a very simple example. Consider, in one dimension, solitons are static domain walls between commensurate domains. When the magnetic module vector changes from Q_c to Q_{ic}, all possible permutations of the locations of solitons lead to the entropy difference. Suppose the incommensurate wave length is slightly smaller than the commensurate one, that is, $\lambda_c - \lambda_{ic} = \delta\lambda$.

doi:10.6342/NTU201901151

Comparing these two phases, it is not hard to see the "wavefront" of incommensurate phase lags behind that of the commensurate one by a short distance. If two "waves" start at a same position with different wavelengths, the two wavefronts "meet" each other when one of them is lag or lead by one wavelength. Assuming after m wavelengths, the commensurate "wavefront" meets the incommensurate one, then the latter would have gone through $m+1$ wavelengths.

Let's consider a one-dimensional lattice with lattice constant a first. The relation between wavelength and magnetic modulation wave vector is $\lambda = \frac{2\pi}{qa} = \frac{1}{Q}$, where a is the lattice constant. Let l be the distance over which commensurate and incommensurate "wave" meet each other, then

$$l = m\lambda_c = m/Q_c$$

and

$$l = (m+1)\lambda_{ic} + \delta w \approx (m+1)/Q_{ic},$$

where δw is the width of a domain wall which is very small compared to λ_{ic}. The contribution of $\delta\omega$ can be ignored. By the equations above one can solve $m = Q_c/(Q_{ic} - Q_c)$. Then

$$l = 1/(Q_{ic} - Q_c), \tag{10.2}$$

which can be viewed as the size of a domain in the incommensurate phase. Our argument of domain size agree with the formula (4.16) suggested by P. Bak and J. von Boehm[58].

Physically, the location of a domain wall is where a soliton occurs. The entropy increases as a soliton is produced so the entropy can be calculated by considering the distribution of solitons. According to the spirit of Gaussian distribution, for a sample of length l, there are n solitons and N sites, the number of microscopic states is $\Omega = \frac{N!}{n!(N-n)!}$. We have the entropy per site

$$\Delta s = k_B \ln \Omega \approx k_B \left[\ln(\frac{N}{N+n}) + \frac{n}{N} \ln(\frac{N}{n} - 1) \right],$$

for n and N are large numbers. The density of soliton is n/N. Hence we have a formula for Δs for one dimensional spin chain

$$\Delta s = \ln(1 + a\delta Q) + a\delta Q \ln(\frac{1}{a\delta Q} - 1), \tag{10.3}$$

where $\delta Q = Q_{ic} - Q_c$.

Now we apply the idea above to CuO. Consider vector $\mathbf{Q} \equiv q_1\mathbf{g}_1 + q_2\mathbf{g}_2 + q_3\mathbf{g}_3$ is parallel to $\mathbf{g}_2$-axis in our magnetic unit cell or b-axis in abc-coordinate.

doi:10.6342/NTU201901151

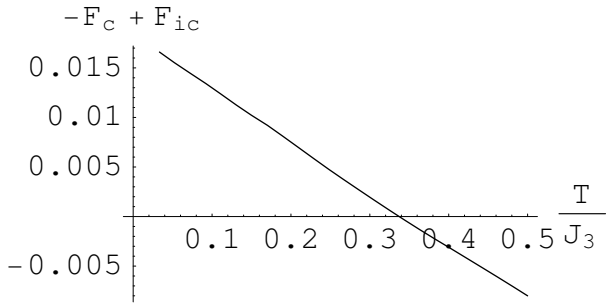

Figure 10.1: The numerical solution of commensurate-incommensurate $T_{c\text{-}ic} \approx 0.337 J_3$

This situation is the same as a one dimensional system because the only direction is given by $\mathbf{Q} = (q_1, 0, q_3)$. Since the entropy is caused by the distribution of solitons, we can think of the wavefront of solitons as moving along ac direction i.e. the hypotenuse of a right triangle. The formula for l has a generalized form

$$l = \sqrt{(1/\delta q_1)^2 + (1/\delta q_3)^2}. \tag{10.4}$$

In the $\mathbf{g}$ coordinate, $\mathbf{Q}_c = \mathbf{g}_3$ and $\mathbf{Q}_{ic} = 0.023\mathbf{g}_1 + 0.989\mathbf{g}_3$. We have $\delta\mathbf{Q} \equiv \mathbf{Q}_{ic} - \mathbf{Q}_c = (0.023, 0, -0.011)$, and the domain length is

$$l = \sqrt{(1/0.023)^2 + (1/0.011)^2} = 100.771.$$

This leads to $n/N \approx 0.01$. So Δs is given by (23):

$$\Delta s = k_B \left[\ln(1 + 0.01) + 0.01 \ln(100.771 + 1)\right] = 0.0557 k_B. \tag{10.5}$$

Since $\mathbf{Q}_c = \mathbf{g}_3$, which is a reciprocal lattice vector of a magnetic unit cell, in $\mathbf{g}$ coordinate representation, the value of Δs in Eq.(10.5) means the entropy per magnetic unit cell. Feeding into Eq.(10.1), FIG. 10.1 shows the numerical solution of critical temperature $T_{c\text{-}ic} \approx 0.337 J_3$. We have explained the spins prefer the commensurate phase at low T in the beginning of this section. As the temperature rises higher than $T_{c\text{-}ic}$, the magnitude of F_{ic} becomes smaller than that of F_c which means the spins are more stable to from incommensurate phase. In many papers of first principle calculation, summarized in [47], the range of the magnitude of $J_3(10\bar{1})$ can be from 50

doi:10.6342/NTU201901151

to 80 meV. We choose $J_3 = 54$ meV, then T_{c-ic} is around 210K, agrees well with the experimental result of *c-ic* phase transition.

The relations in Eq. (10.2) and Eq.(10.3) can in principle be applied to any commensurate-incommensurate systems, especially proper for those of one dimension. First we must know the difference of internal energy and the we measure the wave-vector Q_c and Q_{ic}. Once we have Q_c and Q_{ic} then we can follow the process above to get the transition temperature by the unit of largest spin-spin interaction strength J.

doi:10.6342/NTU201901151

Chapter 11

Conclusion

In chapter 2-6, we consider the exciton condensation of two-dimensional semiconductors. We take germanene as an example but this scheme can also be used in materials of similar type such as silicene. The electron wave functions give rise to a form factor which has profound effect on the symmetry of the gap function. We found that the mixed state has the lowest energy compared to the pure symmetric state and the antisymmetric state. This natural phenomenon is due to the intrinsic SOC interaction and more significantly an external field which can provides a much stronger Rashba interaction in this scenario. The two-dimensional semiconductors also provide a mixed spin state of two types of exciton, known as bright and dark exciton. The measurement of bright exciton can be performed by optical methods. Furthermore, the mixed state solution of condensation can be measure experimentally by probing the midgap states energy in sNp and sNs structures. The former sustains zero-energy midgap states. Finally, the Rashba interaction, no matter how it is generated, by the lattice geometry or by the external field, plays an crucial role in determine the form factors, and hence, the forms of the exciton condensates.

In chapter 7-10, based on the neutron scattering data [44] of CuO, we postulate the spin configuration of the ground state. Using SBMFT, we take two order parameters A and B and diagonalized the Hamiltonian. We derived the energy dispersion and showed the system has finite momentum BEC at $\mathbf{k} = \pm\mathbf{k}_0$. The concept of condensation of quasi-particles (BEC) allows us to explain the finite value of susceptibility in ac direction as T tends to zero. We also analyzed $c - ic$ phase transition. Our model of soliton distribution leads to an entropy difference between commensurate and incommensurate phases. The free energies of two phases are calculated and the critical temperature is found. This results can be compared with experiments and give us a physical picture to consider similar problems. Numerical calculation requires a

doi:10.6342/NTU201901151

lot of computation. The reason is that for an incommensurate system one needs infinite lattice size for a spin to "rotate back". Our argument gives a convincing reason for the entropy consideration without involving heavy numerical calculation.

For the first sight, these two systems are quite different. However, they both exhibited the nature of type II boson condensates as we mentioned in the preface. We practically demonstrated the condensate in detail of type II boson doesn't accompany with superfluidity but with a change of spatial or magnetic order. Generally, for a non-interacting boson system, the BEC happens at $\mathbf{k} = 0$. This fact is shown in exciton condensation at $T = 0$, see Sec. 4.2. In Sec. 8.2 we show a BEC system whose energy dispersion has degenerate minima at two finite momentum $\pm\mathbf{k}_0$. The condensation of Schwinger boson is similar to other kinds of quasi-particles such as spin waves in a lattice (magnons). For bosons consists of quasiparticle such as excitons or magnons. Obviously our SB system coincides with such kind of bosons.

Quasiparticle condensation shows its richness in many aspects. Being as a physical phenomena or a mathematical tool, it offers us a road to deal with many body problems in physics.

doi:10.6342/NTU201901151

Bibliography

[1] *Introduction to Superconductivity* by Michael Tinkham (McGraw Hill; 2nd edition, 1996).

[2] For the books of Bose-Einstein condensation one can refer, for example, *Bose-Einstein Condensation and Superfluidity* by Lev Pitaevskii, Sandro Stringari (Oxford University Press; 1st edition, 2016) or *Bose–Einstein Condensation in Dilute Gases* by C.J. Pethick (Cambridge University Press; 2nd edition, 2011).

[3] M.H. Anderson, J.R. Ensher, M.R. Matthews, C.E. Wieman, and E.A. Cornell. Science., 198–201, (1995).

[4] W. Kohn and D. Sherrington, Rev. Mod. Phys. **42**, 1, (1970).

[5] V. I. Yukalov, Theoret. and Math. Phys., 37:3 (1978), 1093–1101.

[6] Hiroaki T. Ueda and Keisuke Totsuka, Phys. Rev. B **80**, 014417 (2009).

[7] J. Hick, F. Sauli, A. Kreisela and P. Kopietz, Eur. Phys. J. B 78, 429-437 (2010).

[8] arXiv: 0904.3889v1 [cond-mat.quant-gas] (2009).

[9] T. Holstein and H. Primakoff, Phys. Rev. **58**, 1098 (1940)

[10] Massimo Rontani and L.J. Sham, arXiv: 1301.1726 [cond-mat.mes-hall].

[11] Xuejun Zhu, P.B. Littlewood, Mark S. Hybertsen, and T.M. Rice, Phys. Rev. Lett. **74**, 1633 (1995).

[12] Massimo Rontani and L.J. Sham, Phys. Rev. B **80**, 075309 (2009).

[13] See the relevant reviews of in *Bose-Einstein Condensation*, edited by A. Griffin, D.W. Snoke, and S. Stringari (Cambridge University Press, Cambridge, 1995). For even more specific reviews, see *Bose-Einstein*

doi:10.6342/NTU201901151

Condensation of Excitons and Biexcitons: And Coherent Nonlinear Optics with Excitons, by S.A. Moskalenko and D.W. Snoke (Cambridge University Press, Cambridge, 2000).

[14] A.N. Kozlov and L.A. Masksimov, Soviet Phys. JETP **21**, 790 (1965)

[15] L.V. Keldysh and A.N. Kozlov, Soviet Phys. JETP **27**, 521 (1968).

[16] M. Combescot and P. Noisieres, J. Phys C: Solid State Phys, **5**, 2369 (1972).

[17] Y. Naveh and B. Laikhtman, Phys. Rev. Lett. **77**, 900 (1996).

[18] D.I. Pikulin and T. Hyart, Phys. Rev. Lett. **112**, 176403 (2014).

[19] K.S. Novoselov, *et al.*, Science, **306** 666 (2004).

[20] C.C. Liu, W. Feng, and Y. Yao, Phys. Rev. Lett. **107**, 076802 (2011).

[21] Patrick Vogt, *et al.*, Phys. Rev. Lett. **108**, 155501 (2012).

[22] C.L. Kane and E.J. Mele, *et al.*, Phys. Rev. Lett. **95**, 226801 (2005).

[23] Y. Yao, *et al.*, Phys. Rev. B **75**, 041401 (2007).

[24] H. Min, *et al.*, Phys. Rev. B **74**, 165310 (2006).

[25] Lev P. Gor'kov and Emmanuel I. Rashba, Phys. Rev. Lett. **87**, 037004 (2001).

[26] Ke-Chuan Weng and C. D. Hu, *Sci. Rep.* **6**, 29919 (2016).

[27] Cheng-Cheng Liu, Hua Jiang, and Yugui Yao, Phys. Rev. B **84**, 195430 (2011).

[28] Stewart E. Barnes, Jun'ichi Ieda, and Sadamichi Maekawa, *Sci. Rep.* **4**, 4105 (2014)

[29] Junsaku Nitta, Tatsushi Akazaki, and Hideaki Takayanagi, Phys. Rev. Lett **78**, 1335 (1997).

[30] P. Cudazzo, C. Attaccalite, I.V. Tokatly, A. Rubio, Phys. Rev. Lett **104**, 226804 (2010).

[31] Zeyu Jiang, Zhirong, Liu, and Yuanchang Li, Wenhui Duan, Phys. Rev. Lett **118**, 266401 (2017).

doi:10.6342/NTU201901151

[32] E. Hanamura and H. Haug, *Phys. Rep.*, **33** 209 (1977).

[33] The fact of weaker coupling strength between different bands is obtained as we calculating the V^{eff}. Coefficients f's will show this fact. The coupling strength of different bands is proportional to r time f which is about 0.01 times smaller than f.

[34] See the classic book of Schrieffer, *Theory of Superconductivity*, by J.R. Schrieffer (W. A. Benjamin, Inc., 1964)

[35] D. Jerome, T. M. Rice, and W. Kohn, Phys. Rev. **158**, 462 (1967).

[36] Basically, the formula of ground state energy can be found in many textbooks. For example, Philips L.Taylor and Olle Heinonen: *A Quantum Approach to Condensed Matter Physics* (Cambridge University Press, Cambridge, 2002).

[37] The integration area in approximation method is a π^3 disk while in the numerical method is a $4\pi^2$ square.

[38] L.V. Butov and A. I. Filin, Phys. Rev. B **58**, 1980 (1998).

[39] S. Yang, *et al.*, Phys. Rev. Lett. **97**, 187402 (2006).

[40] P.G. de Gennes, *Superconductivity of Metals and Alloys*, (New York, 1966).

[41] Monique Combescot, Odile Betbeder-Matibet, and Roland Combescot, Phys. Rev. Lett. **99**, 176403 (2007)

[42] Chia-Ren Hu, Phys Rev. Lett **72**, 1526 (1994).

[43] S. Asbrink and L-. Norrby, *Acta Cryst.* (1970) **26**, 8.

[44] B. X. Yang, T. R. Thurston, J. M. Tranquada and G. Shirane, Phys. Rev. B **39**, 4343 (1989).

[45] P J Brown, T Chattopadhyay, J B Forsyth, V Nunez and F Tasset, J.Phys Condens. Matter **3**, 4281.

[46] M. Ain, A Menelle, B M Wanklyn and E P Bertaut, J.Phys Condens. Matter **4**, 5327.

[47] T. Kimura, *et al.* Nature (London) **426**, 55 (2003).

doi:10.6342/NTU201901151

[48] Alessio Filippetti and Vincenzo Fiorentini, Phys. Rev. Lett **95**, 2086405 (2005).

[49] Gianluca Giovannetti, *et al.*, Phys. Rev. Lett **106**, 257601 (2011).

[50] Guang Jin, Kun Gao, Cuang-Can Guo, and Lixin He, Phys. Rev. Lett **108**, 187205 (2012).

[51] R. Villarreal *et al.*, arXiv:1205.5299v1, 23 May 2012.

[52] Pierre Toledano *et al.* Phys. Rev. Lett **106**, 026401 (2011).

[53] D.P. Arovas and A. Auerbach, Phys. Rev. B **38**, 316 (1988).

[54] Sanjoy Sarker, C. Jayaprakash, H. R. Krishnamurthy, Micheal Ma, Phys. Rev. B **40**, 5028 (1989).

[55] Condensed Matter Field Theory, 2nd ed. A. Altland and B. Simons, p88.

[56] Ch. Ruegg, N. Cavadini, Furrer A., H.U. Gudel, K. Kramer, H. Matka, A. Wildes, K. Habicht, and P. Vorderwisch. *Nature*, 423:62-65, (2000).

[57] S.O. Demokritov, V.E. Demidov, D. Dzyapko, G.A. Melkov, A.A. Serga, B. Hilldebrands, and Slavin A.N. *Nature*, 443:430 433, (2006).

[58] P. Bak and J. von Boehm, Phys. Rev. B **21**, 5297 (1980)

doi:10.6342/NTU201901151